Electronic Supplementary Material (ESI) for ChemComm.

Supporting information

Controlling azobenzene photoswitching through combined *ortho*-fluorination and –amination

Zafar Ahmed[+], *Antti Siiskonen*[+], *Matti Virkki*, *Arri Priimagi**

Laboratory of Chemistry and Bioengineering, Tampere University of Technology, P.O. Box 541, FI-33101 Tampere, Finland.

E-mail: arri.priimagi@tut.fi

ORCID IDs:

Zafar Ahmed: 0000-0002-4737-6238
Antti Siiskonen: 0000-0003-3718-2031
Matti Virkki: 0000-0003-1340-9297
Arri Priimagi: 0000-0002-5945-9671

Table of Contents:

1. The structures of the synthesized compounds 1 – 9

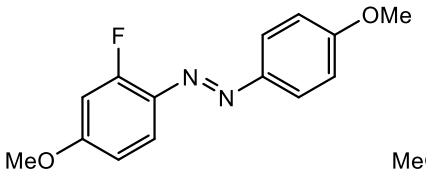

1

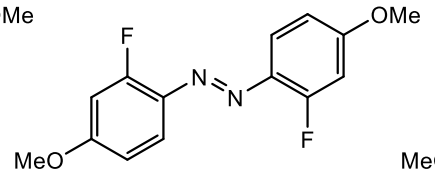

2

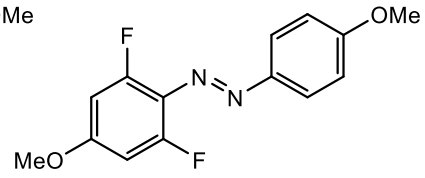

3

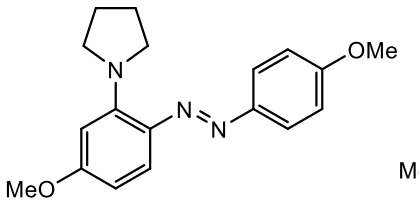

4

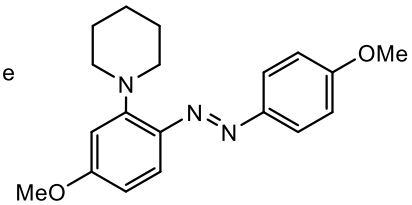

5

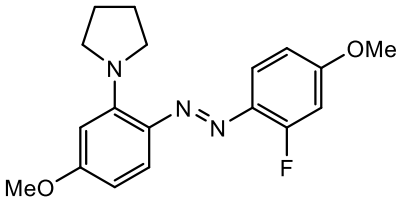

6

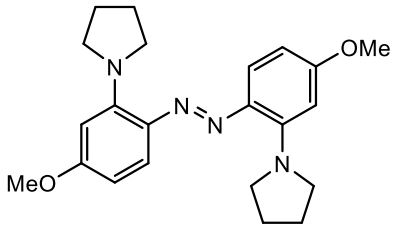

7

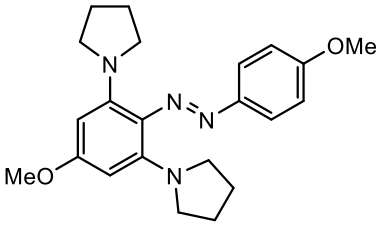

8

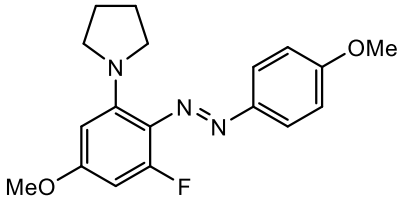

9

2. General Methods

All commercially available reagents and solvents were purchased either from Sigma Aldrich Co. or from VWR and were used without further purifications unless otherwise mentioned. Purification of the products was carried out either by column chromatography on Silica gel 60 (Merck) mesh size 40-63 μm or on preparative TLC plates (Merck) coated with neutral aluminium oxide 60 F254. NMR spectra were recorded using Varian Mercury 300 MHz spectrometer using TMS as internal standard. HRMS measurements were done with Waters LCT Premier XE ESI-TOF bench top mass spectrometer. Lock-mass correction (leucine enkephaline as reference compound), centering and calibration were applied to the raw data to obtain accurate mass. UV-visible absorption spectra were recorded using quartz cuvettes on an

Agilent Cary 60 spectrophotometer equipped with an Ocean Optics qpod 2e Peltier-thermostated cell holder (temperature accuracy ± 0.1 °C). Photoexcitation experiments were conducted using a Prior Lumen 1600 light source with multiple choices for narrow-band LEDs at different wavelengths. The photoexcitation wavelengths were chosen for each compound near an absorption maximum.

3. Synthesis

(*E*)-1-(2-fluoro-4-methoxyphenyl)-2-(4-methoxyphenyl)diazene (1):

To a solution of 3-fluorophenol (3 mmol, 236 mg) and 4-methoxyphenyldiazonium tetrafluoroborate (3.3 mmol, 732 mg) in MeCN (7.5 mL) was added K_2CO_3 (12 mmol, 1.65 g) at room temperature. The reaction mixture turned reddish-brown. After 30 min, another portion of K_2CO_3 (3.0 mmol, 414 mg) and methyl iodide (6 mmol, 360 uL) were added and the mixture was stirred overnight at room temperature. The reaction mixture was diluted with ethyl acetate, filtered through Celite and concentrated on rotary evaporator. The crude was purified by column chromatography on silica gel using 20% ethyl acetate/hexane to yield compound **1** (600 mg, 77%) as orange-yellow solid. ^{1}H NMR (300 MHz, $CDCl_3$, TMS): δ = 7.90 (d, J = 9.09 Hz, 2H), 7.80-7.74 (m, 1H), 6.99 (d, J = 9.09 Hz, 2H), 6.79-6.73 (m, 2H), 3.89 (s, 3H), 3.87 (s, 3H). ^{13}C NMR (75 MHz, $CDCl_3$, TMS): δ = 162.76, 161.86, 160.99 (d, J = 246.02 Hz), 147.29, 134.98 (d, J = 7.19 Hz), 124.65, 118.49 (d, J = 1.66 Hz), 114.16, 110.67 (d, J = 2.76 Hz), 101.84 (d, J = 23.77 Hz), 55.82, 55.55. ^{19}F NMR (282 MHz, $CDCl_3$): δ = -122.34 (m). MS (ESI-TOF): *m/z* calcd for $C_{14}H_{13}FN_2O_2$: 261.1101; found: 261.1039 $[M+H]^+$.

(*E*)-1,2-bis(2-fluoro-4-methoxyphenyl)diazene (2):

Compound **2** was prepared following a reported procedure.[1] A mixture of 2-fluoroaniline (3.61 mmol, 510 mg), freshly ground $KMnO_4$ (1.80 g) and $FeSO_4{\cdot}7H_2O$ (1.80 g) in DCM (36 mL) was refluxed overnight. After cooling to the room temperature, the reaction mixture was filtered through Celite, dried over $MgSO_4$ and concentrated under reduced pressure. The crude residue was purified by column chromatography using 20% ethyl acetate/hexane to give the desired symmetrical azobenzene **3** (350 mg, 35%) as an orange/red solid. ^{1}H NMR (300 MHz, $CDCl_3$, TMS): δ = 7.84-7.78(m, 2H), 6.79-6.73 (m, 4H), 3.88 (s, 3H). ^{13}C NMR (75 MHz, $CDCl_3$, TMS): δ = 163.31 (d, J = 9.40 Hz), 161.50 (d, J = 256.52 Hz), 135.49 (d, J = 7.19 Hz), 118.95 (d, J = 2.21 Hz), 111.01 (d, J = 2.77 Hz), 102.04 (d, J = 23.77 Hz), 56.10. ^{19}F NMR

(282 MHz, $CDCl_3$): δ = -122.07 (m). MS (ESI-TOF): *m/z* calcd for $C_{14}H_{12}F_2N_2O_2$: 279.0943; found: 279.0945 $[M+H]^+$.

(*E*)-1-(2,6-difluoro-4-methoxyphenyl)-2-(4-methoxyphenyl)diazene (3):

Compound **3** was prepared by following the similar procedure used for the synthesis of **1**. To a solution of 3,5-difluorophenol (2 mmol, 262 mg) and 4-methoxyphenyldiazonium tetrafluoroborate (2.2 mmol, 488 mg) in MeCN (5 mL) was added K_2CO_3 (8 mmol, 1.10 g) at room temperature. The reaction mixture turned reddish-brown. After 30 min, another portion of K_2CO_3 (2.0 mmol, 276 mg) and methyl iodide (4 mmol, 240 uL) were added and the mixture was stirred overnight at room temperature. The reaction mixture was diluted with ethyl acetate, filtered through Celite and concentrated on rotary evaporator. The crude was purified by column chromatography on silica gel using 20% ethyl acetate/hexane to yield compound **2** (445 mg, 84%) as orange-yellow solid. ^{1}H NMR (300 MHz, $CDCl_3$, TMS): δ = 7.90 (d, *J* = 9.00 Hz, 2H) , 7.00 (d, *J* = 9.00 Hz, 2H), 6.58 (d, *J* = 9.00 Hz, 2H), 3.90 (s, 3H), 3.86 (s, 3H). ^{13}C NMR (75 MHz, $CDCl_3$, TMS): δ = 162.26, 160.86 (t, *J* = 13.52 Hz), 157. 20 (dd, *J* = 257.87, 7.73 Hz), 147.93, 124.56, 114.16, 98.95 (d, *J* = 2.90 Hz), 98.60 (d, *J* = 1.93 Hz), 56.00, 55.58. ^{19}F NMR (282 MHz, $CDCl_3$): δ = -118.73 (m). MS (ESI-TOF): *m/z* calcd for $C_{14}H_{12}F_2N_2O_2$: 279.0928; found: 279.0945 $[M+H]^+$.

(*E*)-1-(5-methoxy-2-((4-methoxyphenyl)diazenyl)phenyl)pyrrolidine (4):

A mixture of compound **1** (0.115 mmol, 30 mg) and pyrrolidine (2 mL) was stirred at room temperature for 6 hours. The reaction mixture was diluted with ethyl acetate (20 mL). The organic phase was washed with water (3×), dried over Na_2SO_4 and concentrated. The crude was purified over silica gel using ethyl acetate/hexane (20%) as eluent to yield compound **4** (32 mg, 90%) as dark orange solid.^{1}H NMR (300 MHz, $CDCl_3$, TMS): δ = 7.80 (d, *J* = 9.00 Hz, 1H), 7.75 (d, *J* = 9.00 Hz, 2H), 6.99 (d, *J* = 9.00 Hz, 2H), 6.34-6.29 (m, 2H), 3.88 (s, 3H), 3.86 (s, 3H), 3.70-3.26 (m, 4H), 2.03-1.99 (m, 4H). ^{13}C NMR (75 MHz, $CDCl_3$, TMS): δ = 162.52, 160.22, 148.28, 147.86, 135.54, 123.76, 118.22, 114.06, 103.50, 99.39, 55.49, 55.27, 52.42, 25.93. MS (ESI-TOF): *m/z* calcd for $C_{18}H_{21}N_3O_2$: 312.1716; found: 312.1712 $[M+H]^+$.

(*E*)-1-(5-methoxy-2-((4-methoxyphenyl)diazenyl)phenyl)piperidine (5):

A mixture of compound **1** (0.096 mmol, 25 mg) and pyrrolidine (2 mL) was stirred at 55 ˚C for 20 hours. The reaction mixture was cooled to room temperature and diluted with ethyl acetate (20 mL). The organic phase was washed with water (3×), dried over Na_2SO_4 and

concentrated. The crude product was purified over silica gel using ethyl acetate/hexane (20%) as eluent to yield compounds **5** (30 mg, 96 %) as dark orange solid. ^{1}H NMR (300 MHz, $CDCl_3$, TMS): δ = 7.90 (d, *J* = 9.00 Hz, 2H) , 7.69 (d, *J* = 6.00 Hz, 1H), 7.00 (d, *J* = 9.00 Hz, 2H), 6.59-6.52 (m, 2H), 3.89 (s, 3H), 3.86 (s, 3H), 3.23-3.19 (m, 4H), 1.87-1.79 (m, 4H), 1.68-1.60 (m, 2H). ^{13}C NMR (75 MHz, $CDCl_3$, TMS): δ = 162.65, 161.41, 153.23, 147.79, 139.26, 124.56, 118.28, 114.36, 106.57, 104.50, 55.76, 55.63, 54.74, 26.59, 24.63. MS (ESI-TOF): *m/z* calcd for $C_{19}H_{23}N_3O_2$: 326.1848; found: 326.1869 $[M+H]^+$.

(*E*)-1-(2-((2-fluoro-4-methoxyphenyl)diazenyl)-5-methoxyphenyl)pyrrolidine (6): A mixture of compound **2** (0.089 mmol, 25 mg) and pyrrolidine (2 mL) were stirred at room temperature for 20 hours. The reaction mixture was diluted with ethyl acetate (20 mL). The organic phase was washed with water (3×), dried over Na_2SO_4 and concentrated. The crude was purified over silica gel using ethyl acetate/hexane (20%) as eluent to yield compound **6** (24 mg, 81 %) and **7** (5 mg, 15%) as dark orange solids respectively. ^{1}H NMR (300 MHz, $CDCl_3$, TMS): δ = 7.85 (d, *J* = 9.00 Hz, 1H), 7.58-7.52 (m, 1H), 6.78-6.70 (m, 2H), 6.32-6.25 (m, 2H), 3.85 (s, 6H), 3.69-3.64 (m, 4H), 2.03-1.98 (m, 4H). ^{13}C NMR (75 MHz, $CDCl_3$, TMS): δ = 163.13, 161.29 (d, J = 10.50 Hz), 160.42 (d, J = 252.66 Hz), 148.78, 136.21, 136.05 (d, J = 6.63 Hz), 118.90, 118.80 (d, J = 2.76 Hz), 110.70 (d, J = 3.32 Hz), 104.14, 102.08 (d, J = 23.77 Hz), 99.44, 56.00, 55.52, 52.70, 26.17. ^{19}F NMR (282 MHz, $CDCl_3$): δ = -123.17 (m). MS (ESI-TOF): *m/z* calcd for $C_{18}H_{20}FN_3O_2$: 330.1602; found: 330.1618 $[M+H]^+$.

(*E*)-1,2-bis(4-methoxy-2-(pyrrolidin-1-yl)phenyl)diazene (7): A mixture of compound **3** (0.071 mmol, 20 mg) and pyrrolidine (2 mL) was stirred at 55 ˚C for 20 hours. The reaction mixture was cooled to room temperature and diluted with ethyl acetate (20 mL). The organic phase was washed with water (3×), dried over Na_2SO_4 and concentrated. The crude product was purified over silica gel using ethyl acetate/hexane (20%) as eluent to yield compounds **6** (6 mg, 21 %) and **7** (20 mg, 74%) as dark orange solids. **Compound 7:** ^{1}H NMR (300 MHz, $CDCl_3$, TMS): δ = 7.59 (d, *J* = 9.68 Hz, 2H), 6.34-6.30 (m, 4H), 3.85 (s, 6H), 3.69-3.65 (m, 8H), 2.02-1.98 (m, 8H). ^{13}C NMR (75 MHz, $CDCl_3$, TMS): δ = 161.56, 148.01, 136.71, 118.41, 103.15, 100.00, 55.50, 52.70, 26.16. MS (ESI-TOF): *m/z* calcd for $C_{22}H_{28}N_4O_2$: 381.2296; found: 381.2291$[M+H]^+$.

(*E*)-1,1'-(5-methoxy-2-((4-methoxyphenyl)diazenyl)-1,3-phenylene)dipyrrolidine (8): A mixture of compound **3** (0.093 mmol, 26 mg) and pyrrolidine (2 mL) was stirred at room temperature for 6 hours. The reaction mixture was diluted with ethyl acetate (20 mL). The

organic phase was washed with water (3×), dried over Na_2SO_4 and concentrated. The crude was purified over silica gel using ethyl acetate/hexane (20%) as eluent to yield compound **8** (10 mg, 28%) as dark orange solid. The compound **6** was very labile as degradation was already observed during purification and characterization.^{1}H NMR (300 MHz, $CDCl_3$, TMS): δ = 7.65 (d, *J* = 8.78 Hz, 2H), 6.5 (d, *J* = 8.78 Hz, 2H), 5.81 (s, 2H), 3.86 (s, 3H), 3.84 (s, 3H), 3.40-3.35 (m, 8H), 1.94-190 (m, 8H). 13C NMR (75 MHz, $CDCl_3$, TMS): δ = 162.38, 159.19, 148.87, 148.40, 122.61, 113.97, 113. 86, 88.97 (d, *J* = 4.61 Hz), 55.52-55.03 (m), 52.42, 25.82. MS (ESI-TOF): *m/z* calcd for $C_{22}H_{28}N4O_2$: 381.2263; found: 381.2291$[M+H]^+$.

(*E*)-1-(3-fluoro-5-methoxy-2-((4-methoxyphenyl)diazenyl)phenyl)pyrrolidine (9):

To a solution of compound **3** (0.2 mmol, 53 mg) in MeCN (2 mL) was added pyrrolidine (1 mmol, 80 uL) dropwise at room temperature. After 2.5 h, the reaction mixture was diluted with EtOAc (25 mL), washed with saturated $NaHCO_3$ (15 mL), dried over Na_2SO_4, filtered and evaporated. The crude was purified over silica gel using 5% ethyl acetate/toluene as eluent to yield compound **9** (61 mg, 92%) as an orange solid. ^{1}H NMR (300 MHz, $CDCl_3$, TMS): δ = 7.78 (d, *J* = 9.00 Hz, 2H), 6.99 (d, *J* = 9.00 Hz, 2H), 6.13-6.03 (m, 2H), 3.88 (s. 3H), 3.82 (s, 3H), 3.51-3.47 (m, 4H), 1.96-1.91 (m, 4H). ^{13}C NMR (75 MHz, $CDCl_3$, TMS): δ = 161.06, 160.61 (d, *J* = 14.49 Hz), 154.30 (d, *J* = 256.90), 148.16, 148.09, 148.07 (m), 125.66 (d, J = 7.73 Hz), 123.76, 114.13, 114.04, 95.55 (d, J = 1.93 Hz), 91.39, 91.06, 55.55-55.37 (m), 52.47, 25.82. ^{19}F NMR (282 MHz, $CDCl_3$): δ = -122.05 (m). MS (ESI-TOF): *m/z* calcd for $C_{18}H_{20}FN_3O_2$: 330.1635; found: 330.1618 $[M+H]^+$.

4. Computational studies

All the calculations were performed with Gaussian 16 Revision A.03 (Gaussian Inc., Wallingford CT). The B3LYP/6-31+G(d,p) method was used and the calculations were performed in acetonitrile using the polarizable continuum model (PCM). Default values were used for other parameters. A frequency calculation was performed after each geometry optimization to conform that the obtained conformation was a true minimum (*i.e.* no imaginary frequencies) or a transition state (one imaginary frequency). Intrinsic reaction coordinate (IRC) runs were used to verify that the obtained transition states lead to starting materials and products.

The density functional theory calculations, used to gain further insight into the reaction mechanism and selectivity, revealed that the azo group could act either as a base or as a hydrogen-bond acceptor, thereby leading to two different reaction mechanisms (see below). Reaction of **1** with piperidine and that of **3** and **9** with pyrrolidine proceeds via three-step mechanism. The initial transition state leads to an intermediate with the proton still attached to the amine nitrogen. This proton migrates to the azo group and cleavage of fluorine in the final step affords the desired product. Compounds **1**, **2** and **6** react with pyrrolidine via a one-step mechanism where the initial transition state directly leads to the final product and the azo group acts only as a hydrogen-bond acceptor, not as a base. In both mechanisms, the attack by amine is the rate-determining step. The selectivity can be explained by comparing the energy barriers for that step (Table S1). As expected, the electron-withdrawing fluorine in **3** clearly decreases the energy barrier, or increases the reaction rate. The second amination of the resulting product (**9** → **8**) is much slower, presumably due to steric hindrance and the electron-donating effect of the pyrrolidine substituent. A fluorine on the opposite ring, as in **2**, does not have a significant effect on the energy barrier. However, the presence of an amine on the opposite ring, as in **6**, increases the energy barrier significantly, presumably due to steric effects.

Table S1. The amination reaction energy barriers (ΔE) and changes in free energies (ΔG) for the transition states (in kcal mol^{-1}) (B3LYP/6-31+G(d,p)) in acetonitrile (PCM).

Reaction	ΔE[a]	ΔE relative to **1 → 4**	ΔG[a]	ΔG relative to **1 → 4**
1 → 4	17.0	0	32.9	0
1 → 5	24.1	7.1	39.3	6.4
2 → 6	17.3	0.3	33.2	0.3
6 → 7	22.6	5.6	36.6	3.7
3 → 9	15.2	-1.8	30.9	-2.0
9 → 8	20.1	3.1	34.4	1.5

[a] Relative to the sum of starting materials

Transition states:

The transition states were located using the command "opt(ts,calcfc)" and the starting geometry for the calculations were chosen by running a constrained geometry scan and varying the relevant interatomic distance (Figure S1). The geometry with the highest energy was chosen as the starting geometry. The scan **A** was used to locate the starting geometry for the first reaction step, **B** for the proton transfer step and **C** for the fluorine cleavage step.

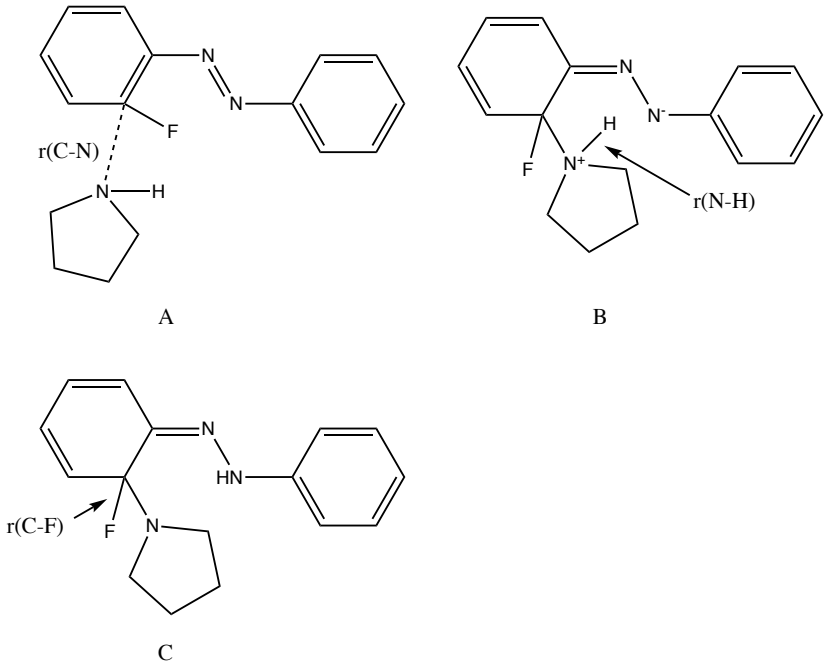

Figure S1. Constrained geometry scans. The interatomic distance that is varied is marked with r(x-x).

One-step vs three-step mechanism:

The proposed one-step (starting material → product) and three-step reaction (starting material → intermediate 1 → intermediate 2 → product) mechanisms are shown in Figure S2.

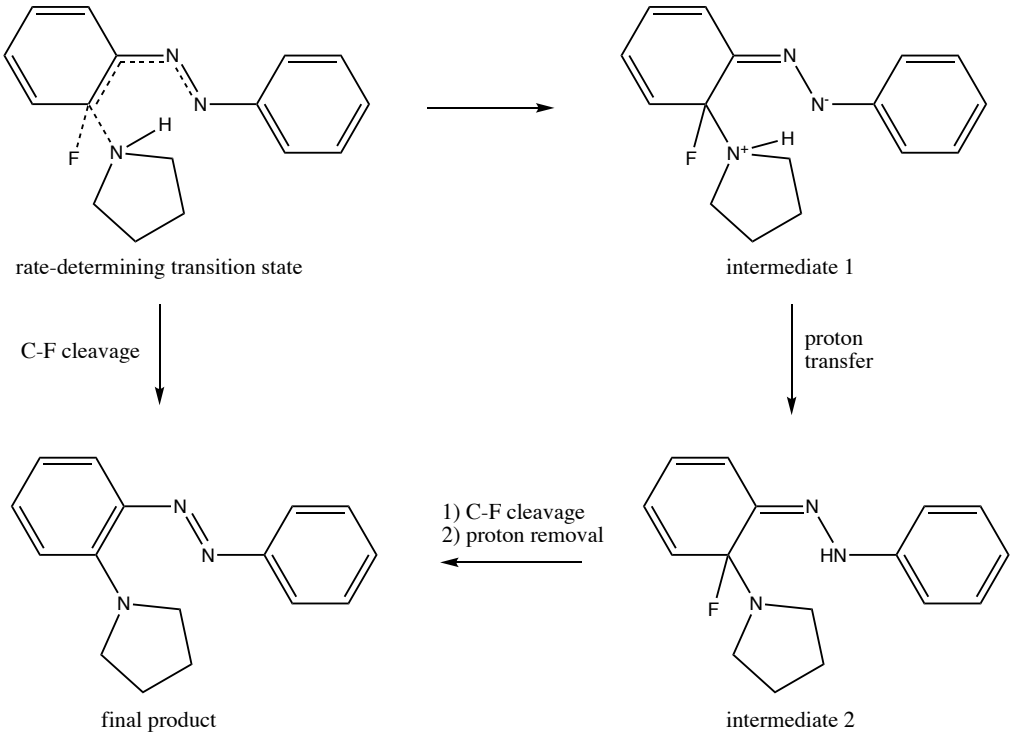

Figure S2. Proposed reaction mechanisms of the amination reaction.

In the one-step mechanism, the first transition state leads directly to the final product by fluorine cleavage. In that case, the azo group functions as a coordinating group via a hydrogen bond, not as a base.

In the three-step mechanism, the first transition state leads to the intermediate 1 where the proton is still attached to pyrrolidine. The proton is then transferred to the azo group via another transition state with a very low energy barrier. The fluorine cleavage then proceeds via a third transition state, which also has a low energy barrier. Finally, the azo group is (presumably) deprotonated by excess pyrrolidine to afford the final product (that step was not modelled)

Transition states and intermediates for the amination of 1-3, 6 and 9:

Reaction 1 → 4: The amination reaction of compound **1** with pyrrolidine proceeds in one-step. The transition state geometry is shown in Figure S3. The IRC run from that transition state led to a geometry similar to intermediate 1 but the subsequent geometry optimization led to the final product, not intermediate 1. The transition state for the proton transfer could be located by starting the constrained geometry optimization from the intermediate 2 (not from the intermediate 1 as for other compounds) but the IRC run backwards from that transition state, which should lead to the intermediate 1, leads to the final product. This odd behavior might be explained by a bifurcated transition state but that idea was not further studied.

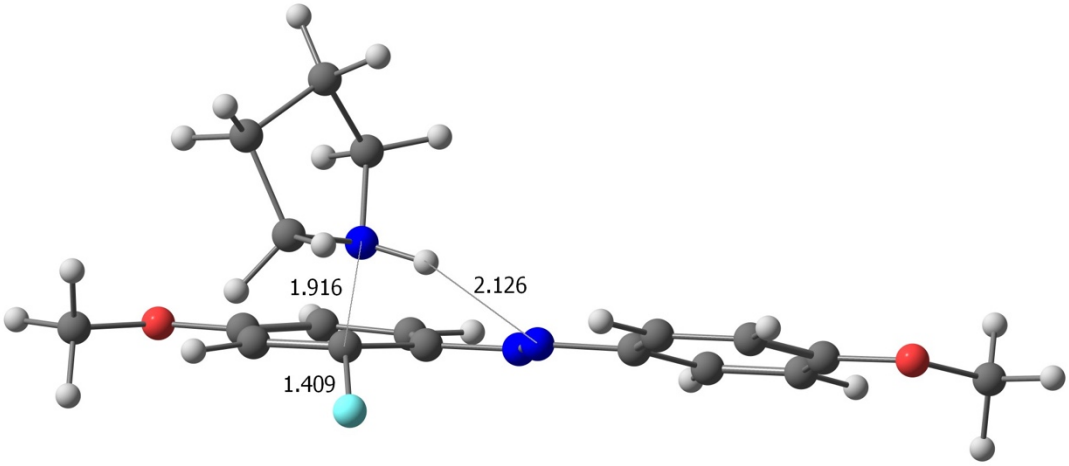

Figure S3. Reaction **1 → 4**: transition state geometry.

Reaction 1 → 5: The amination reaction of **1** with piperidine proceeds in three steps. The transition state for the first step is shown in Figure S4 and the energy barrier is +24.1 kcal/mol. The intermediate 1 is shown in Figure S5 and the energy is +13.0 kcal/mol compared to the starting materials. The transition state for the proton transfer is shown in Figure S6 and the energy is +8.1 kcal/mol. The intermediate 2 is shown in Figure S7 and the energy is +6.2 kcal/mol compared to the starting materials. The transition state for the final step, or the fluorine cleavage is shown in Figure S8 and the energy barrier is +4.1 kcal/mol.

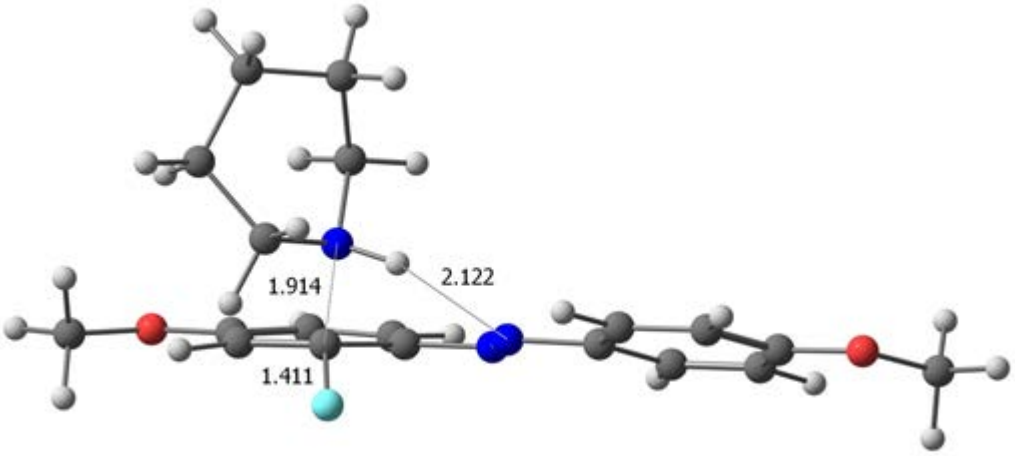

Figure S4. Reaction **1** → **5**: transition state geometry for the first step.

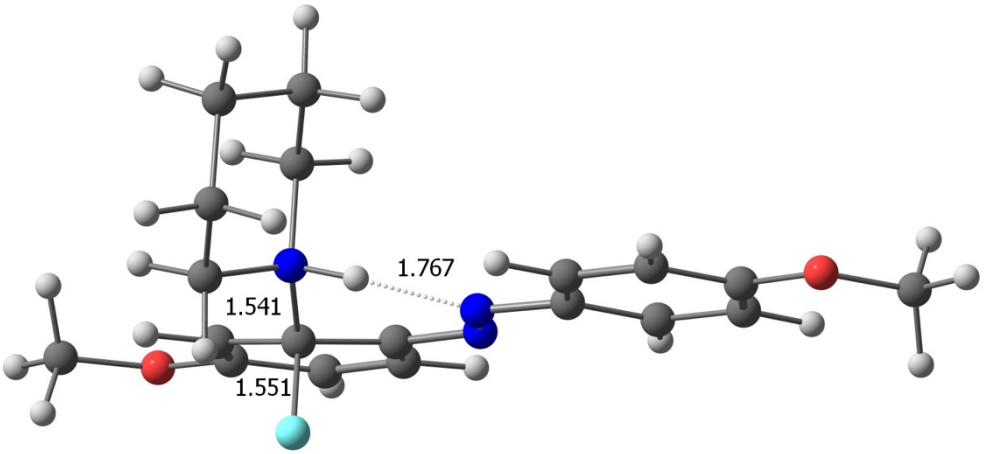

Figure S5. Reaction **1** → **5**: optimized geometry of the intermediate 1.

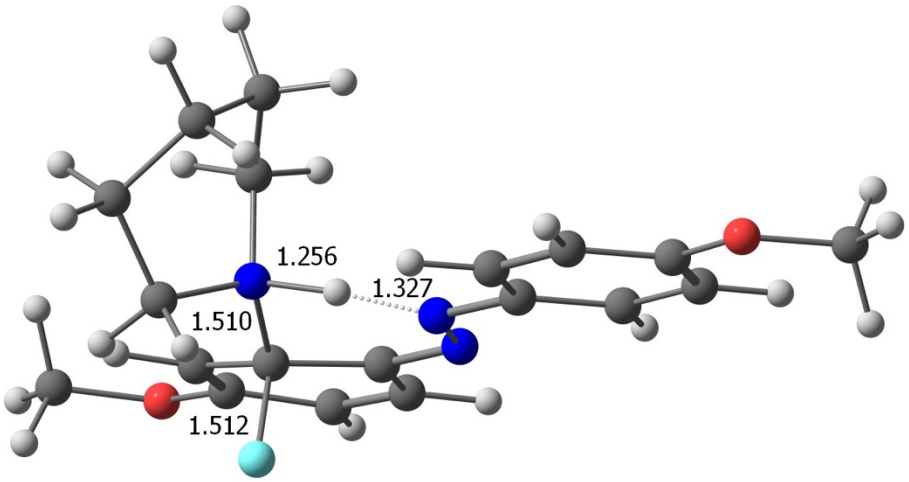

Figure S6. Reaction **1** → **5**: transition state geometry for the proton transfer step.

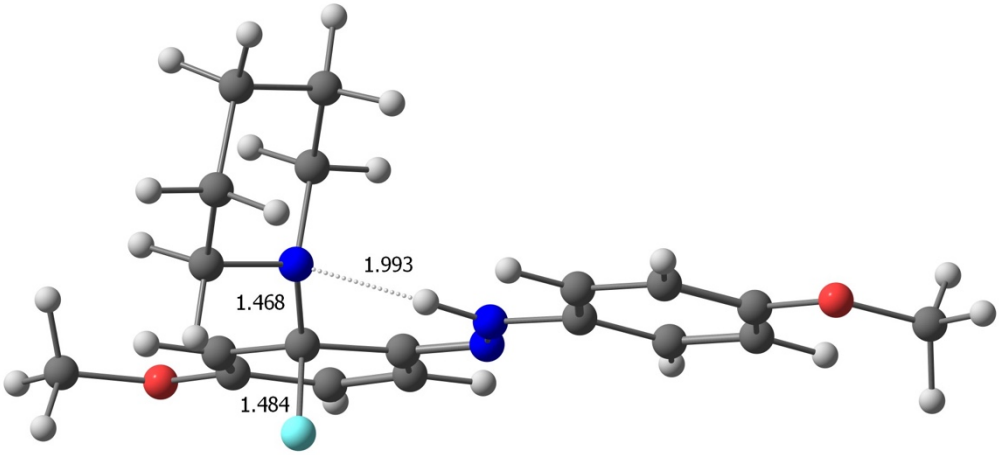

Figure S7. Reaction **1** → **5**: optimized geometry of the intermediate 2.

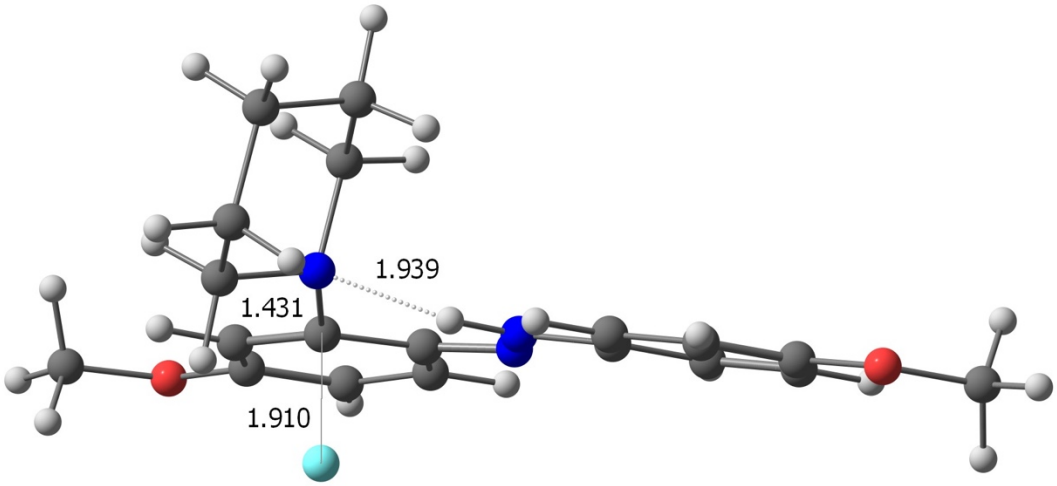

Figure S8. Reaction **1** → **5**: transition state geometry for the fluorine cleavage step.

Reaction 2 → **6**: The amination reaction of **2** proceeds in one step. The transition state is shown in Figure S9 and the energy barrier for that step is +17.0 kcal/mol. The IRC run forward of this transition state leads directly to the final product by cleavage of the fluorine and without the transfer of the proton. Therefore, in this case the azo group acts only as a hydrogen bond acceptor, not as a base.

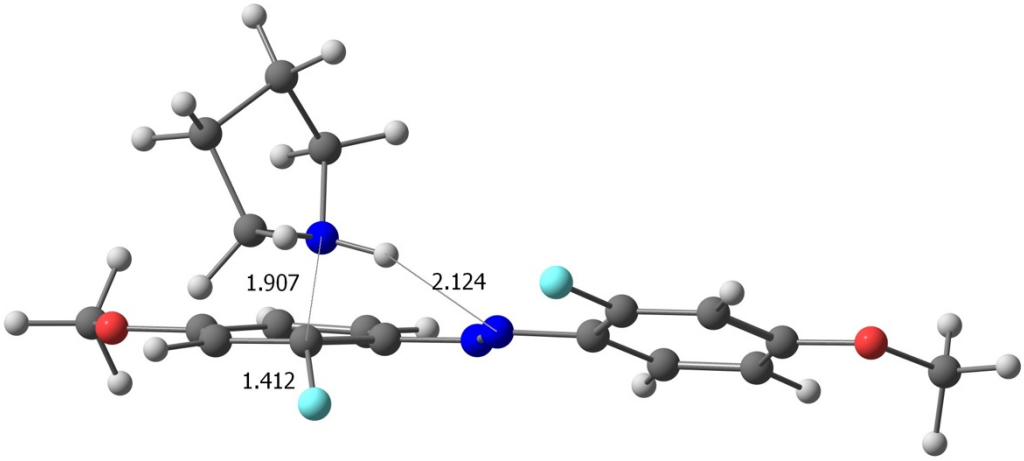

Figure S9. Reaction **2** → **6**: transition state geometry.

Reaction 6 → **7**: The amination reaction of **6** proceeds in one-step. The transition state is shown in Figure S10 the energy barrier is +22.6 kcal/mol. The IRC run forward of that transition state leads directly to the final product without the proton transfer. Therefore, in this case the azo group acts only as a hydrogen bond acceptor, not as a base.

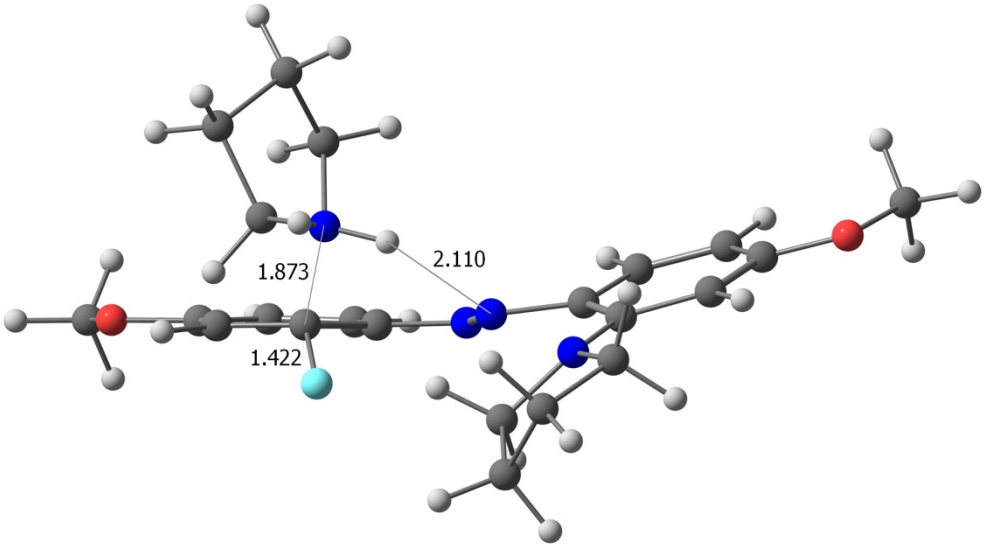

Figure S10. Reaction **6** → **7**: transition state geometry.

Reaction 3 → 9: The amination reaction of **3** proceeds in three steps. The transition state for the first step is shown in Figure S11 and the energy barrier is 15.2 kcal/mol. The intermediate 1 is shown in Figure S12 and the energy is +9.1 kcal/mol compared to starting materials. The transition state for the proton transfer step is shown in Figure S13 and the energy barrier is only 2.4 kcal/mol. The intermediate 2 is shown in Figure S14 and the energy is +3.9 kcal/mol compared to the starting materials. The transition state for the final step, or fluorine cleavage, is shown in Figure S15. The energy barrier for that step is 4.7 kcal/mol.

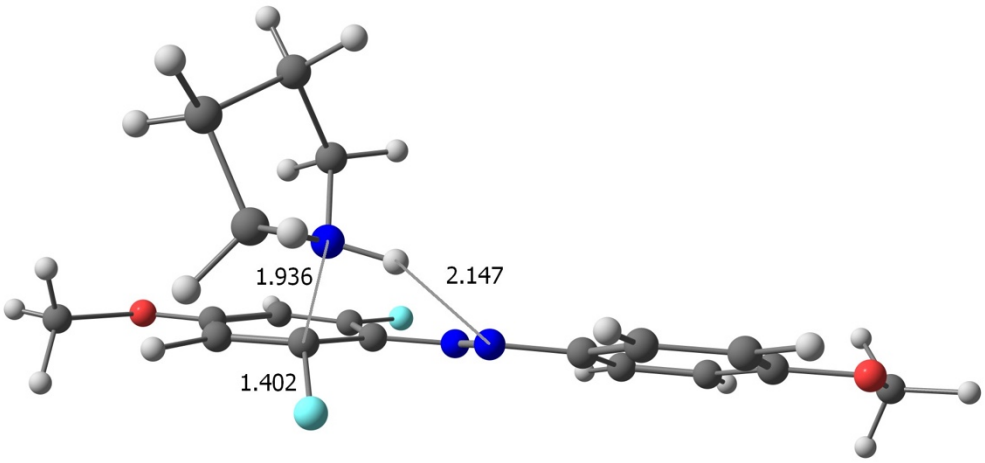

Figure S11. Reaction **3 → 9**: transition state geometry for the first step.

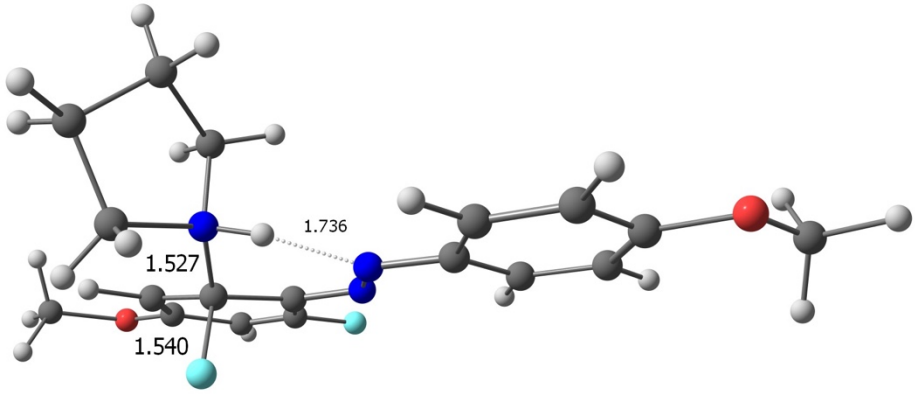

Figure S12. Reaction **3 → 9**: optimized geometry of the intermediate 1.

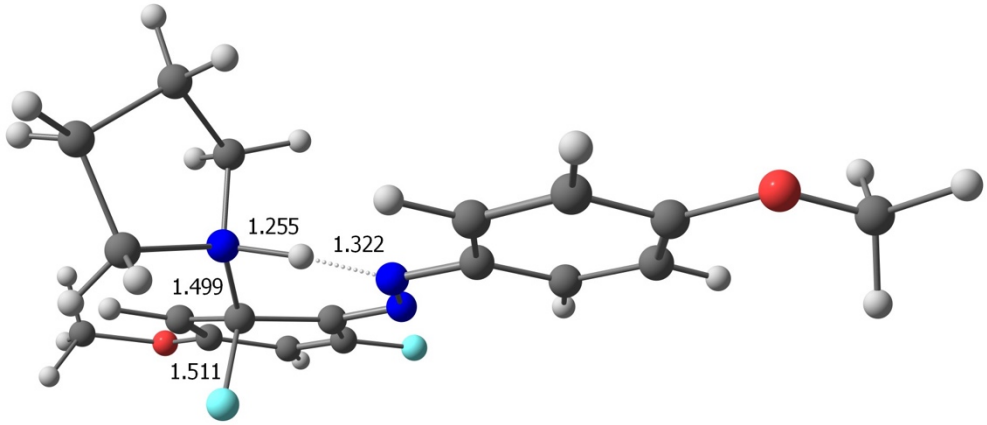

Figure S13. Reaction **3** → **9**: transition state geometry for the proton transfer step.

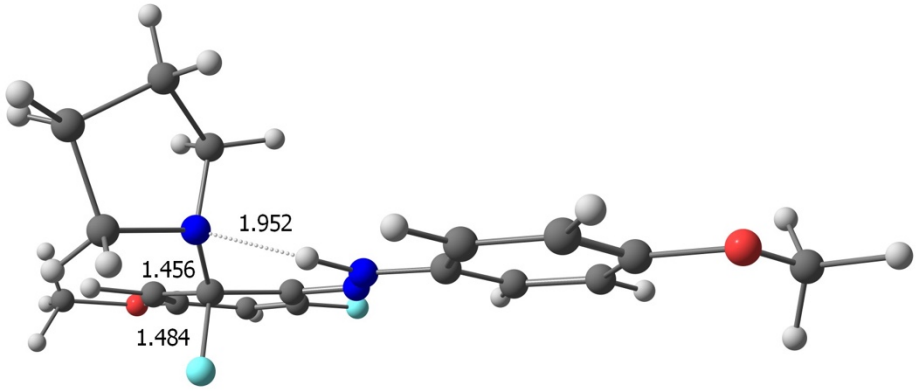

Figure S14. Reaction **3** → **9**: optimized geometry of the intermediate 2.

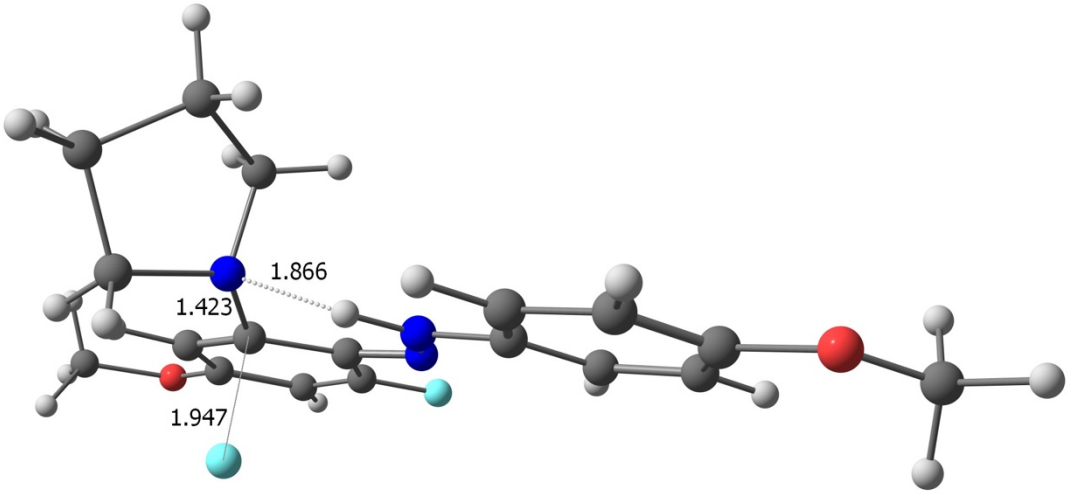

Figure S15. Reaction **3** → **9**: transition state geometry for the fluorine cleavage step.

Reaction 9 → 8: The amination reaction of **9** proceeds in three steps. The transition state for the first step is shown in Figure S16 and the energy barrier is +20.1 kcal/mol. The intermediate 1 is shown in Figure S17 and the energy is +13.6 kcal/mol compared to the starting materials. The transition state for the proton transfer is shown in Figure S18 and the energy barrier is only +1.2 kcal/mol. The intermediate 1 is shown in Figure S19 and the energy is +6.0 kcal/mol compared to the starting materials. The transition state for the final step, or the fluorine cleavage, is shown in Figure S20 and the energy barrier is only +1.9 kcal/mol.

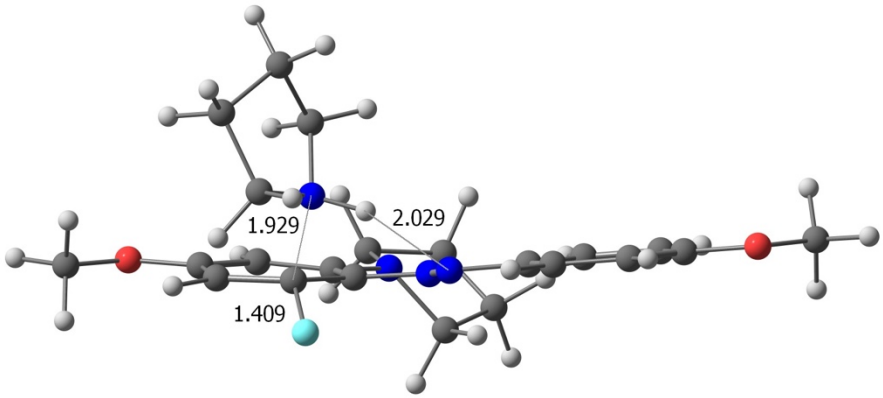

Figure S16. Reaction **9 → 8**: transition state geometry for the first step.

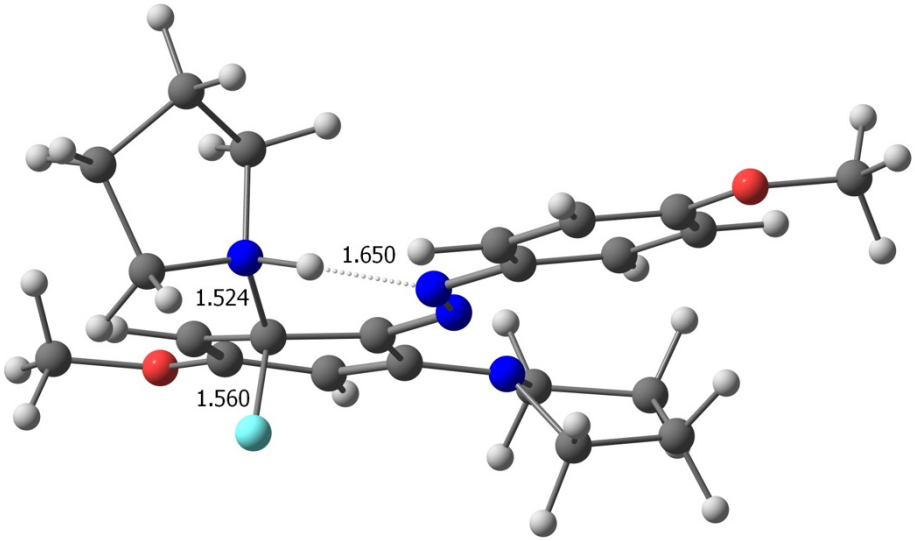

Figure S17. Reaction **9 → 8**: optimized geometry of the intermediate 1.

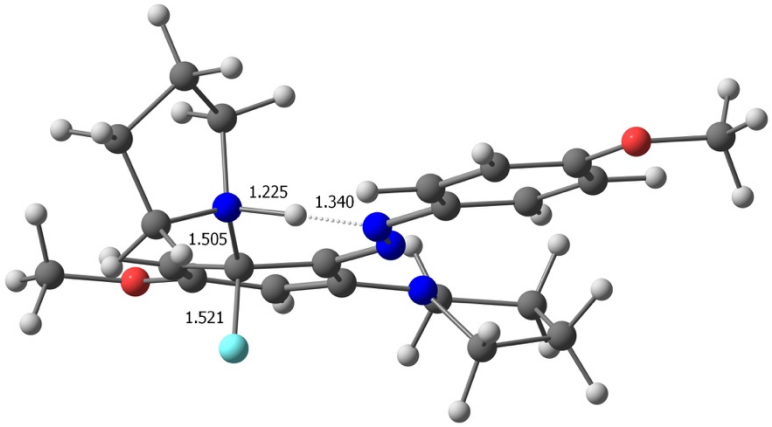

Figure S18. Reaction **9** → **8**: transition state geometry for the proton transfer step.

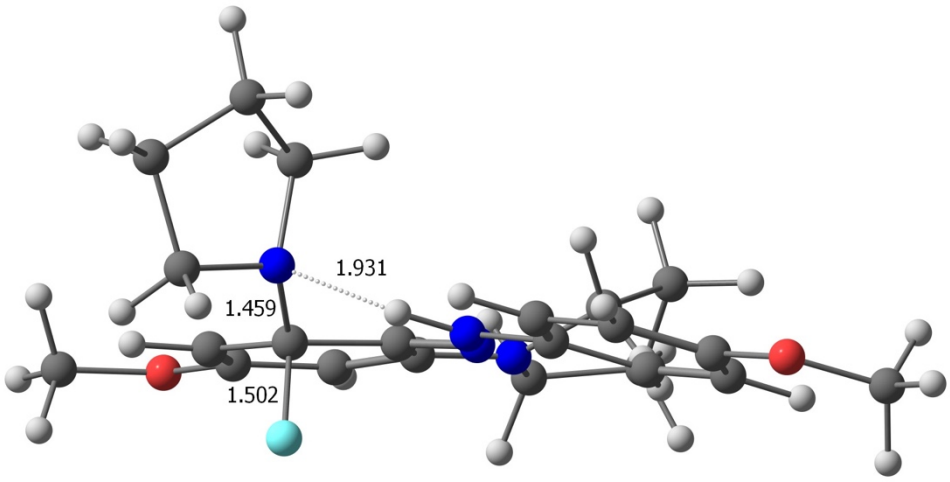

Figure S19. Reaction **9** → **8**: optimized geometry of the intermediate 2.

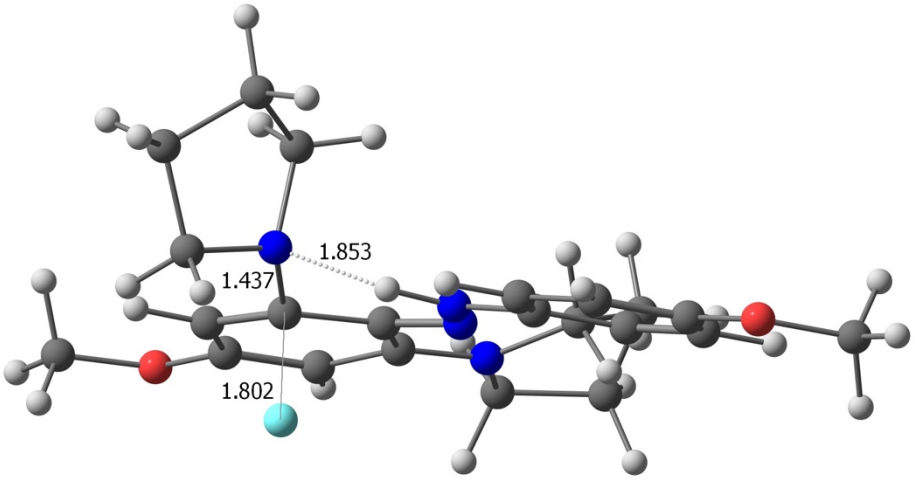

Figure S20. Reaction **9** → **8**: transition state geometry for the fluorine cleavage step.

5. NMR spectra

Compound **1**

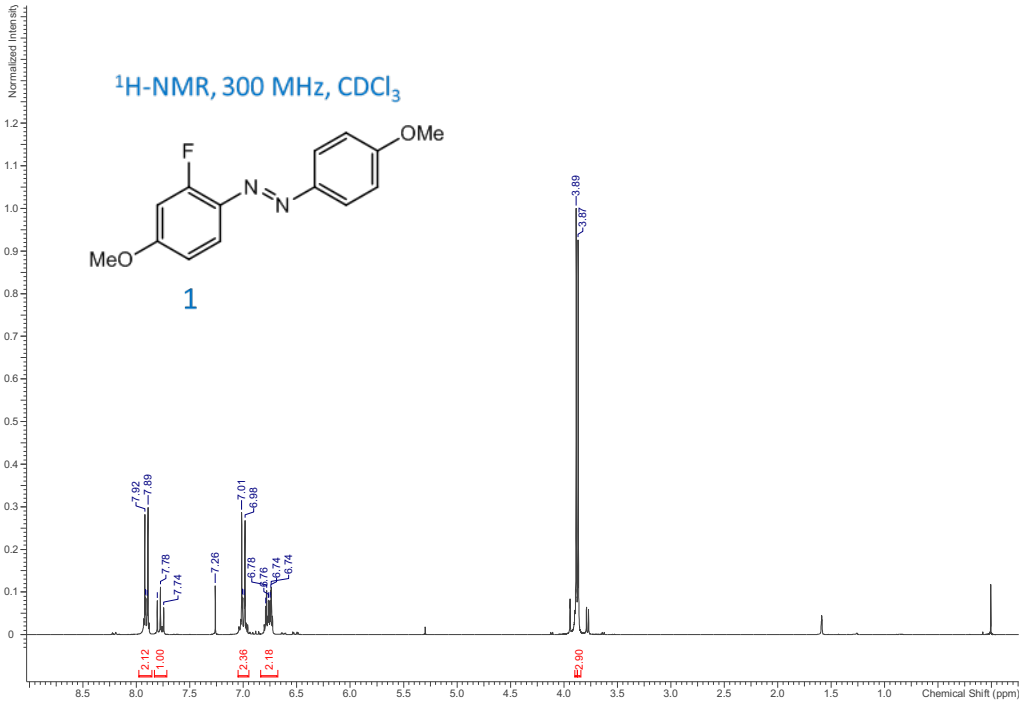

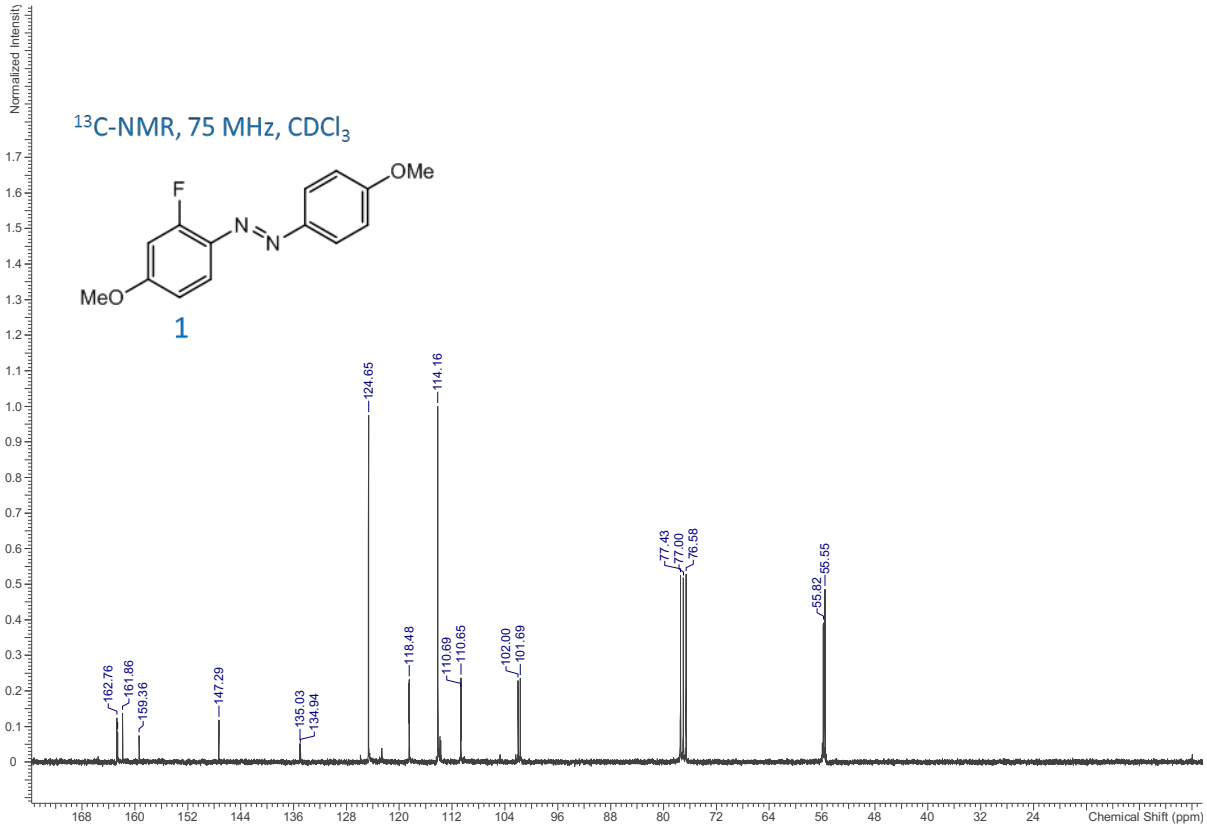

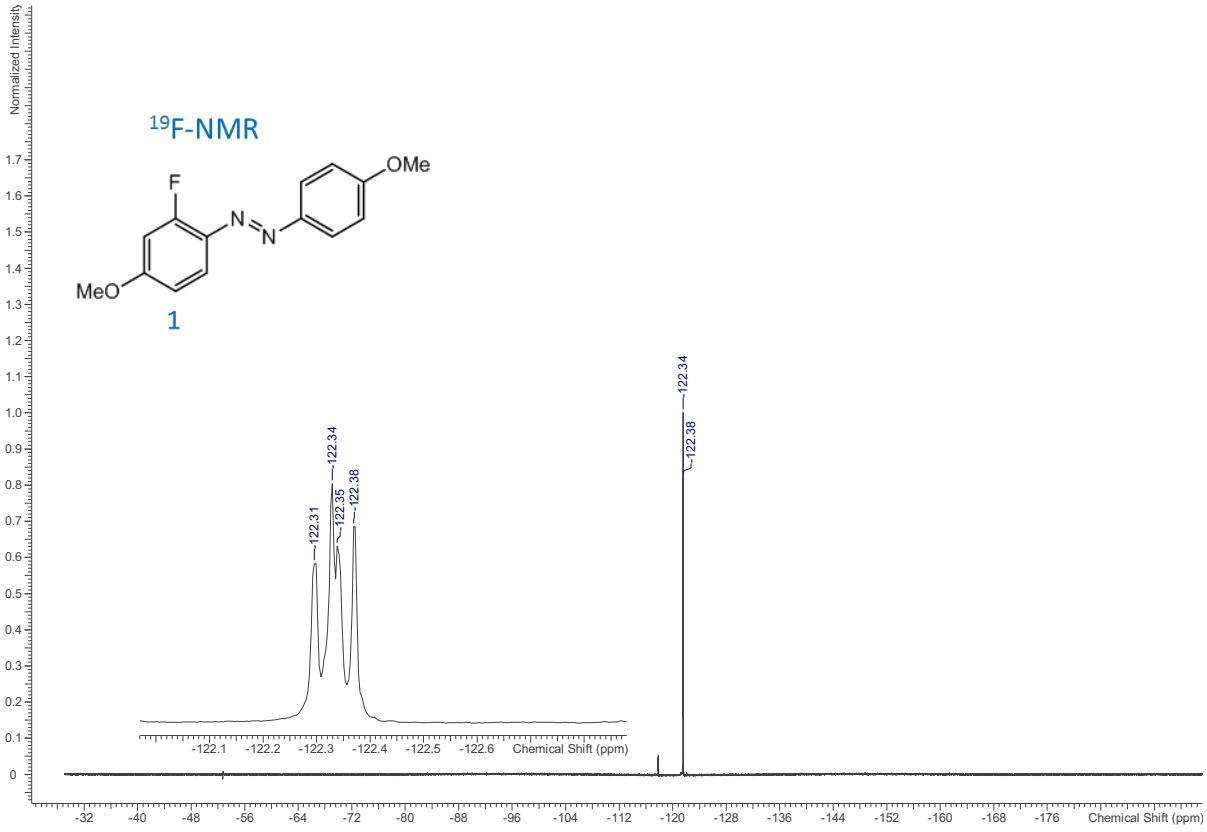
19F-NMR
F
N
N
OMe
MeO
1
Normalized Intensity
122.34
122.38
122.31
122.34
122.35
122.38
Chemical Shift (ppm)

Compound **2**

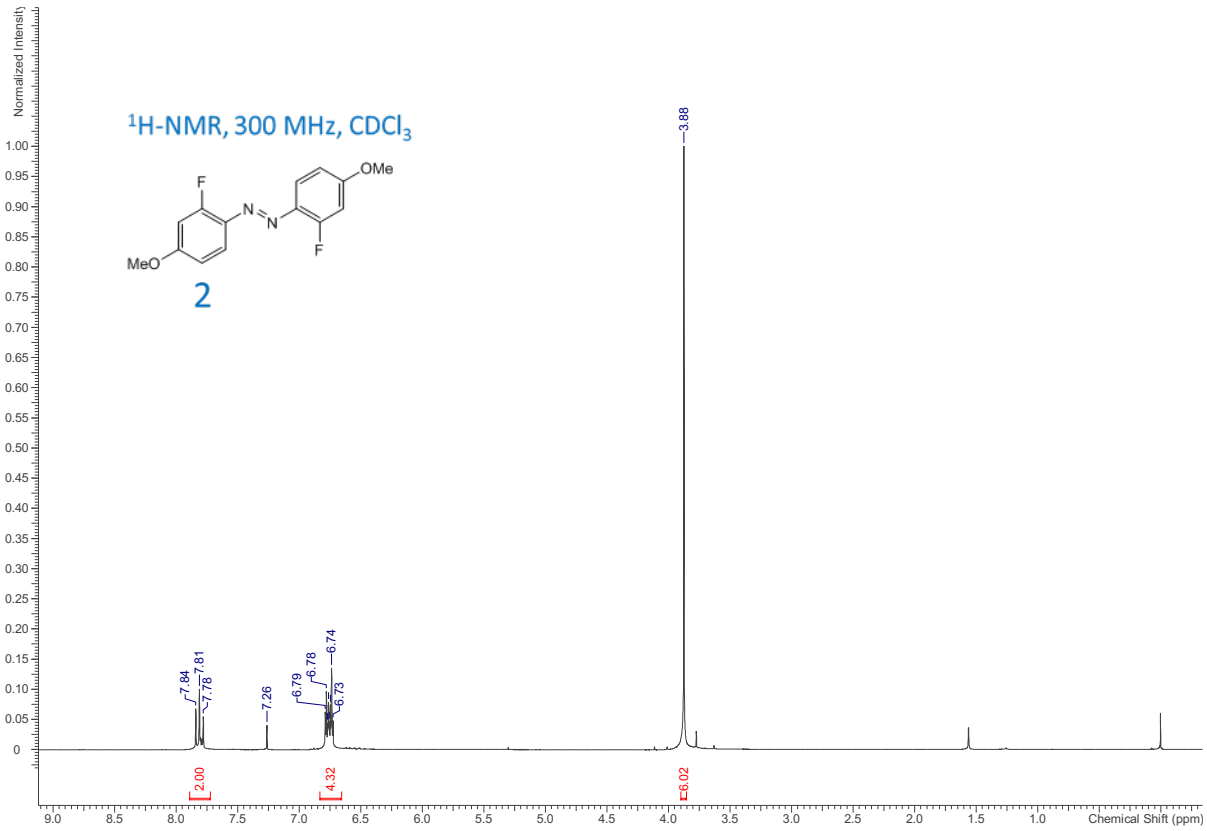
1H-NMR, 300 MHz, CDCl3
F
N
N
OMe
F
MeO
2
Normalized Intensity
3.88
7.84
7.81
7.78
7.26
6.79
6.78
6.74
6.73
2.00
4.32
6.02
Chemical Shift (ppm)

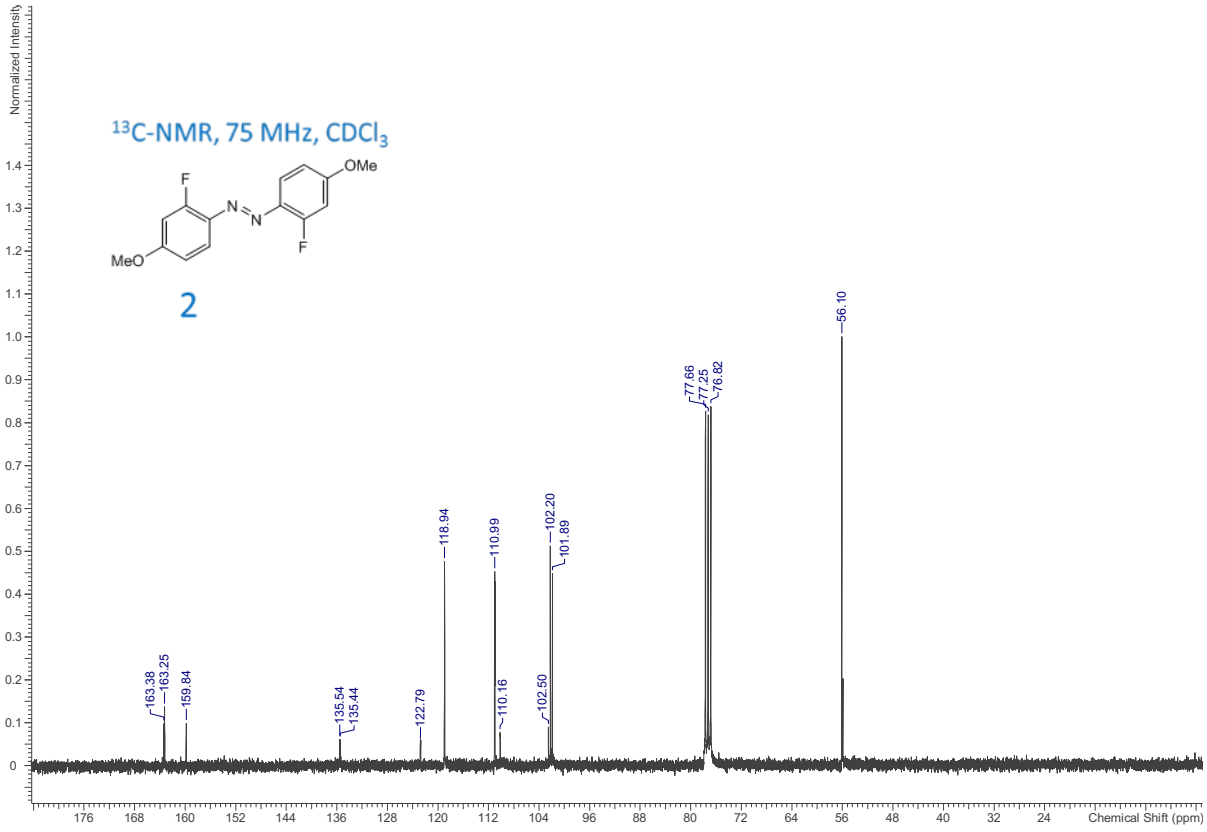
13C-NMR, 75 MHz, CDCl3
F
N
N
OMe
MeO
F
2
Normalized Intensity
163.38
163.25
159.84
135.54
135.44
122.79
118.94
110.99
110.16
102.50
102.20
101.89
77.66
77.25
76.82
56.10
Chemical Shift (ppm)

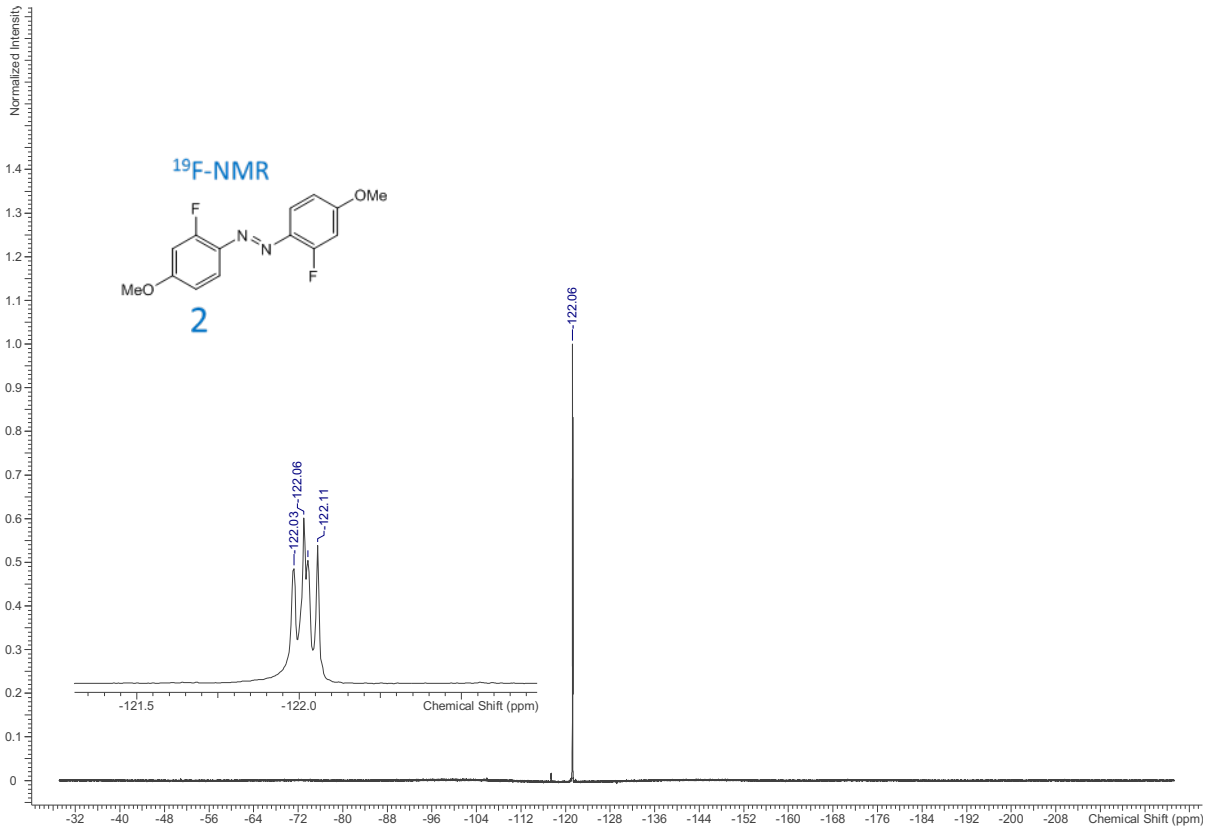
19F-NMR
F
N
N
OMe
MeO
F
2
Normalized Intensity
122.06
122.03
122.06
122.11
-121.5
-122.0
Chemical Shift (ppm)
Chemical Shift (ppm)

Compound **3**

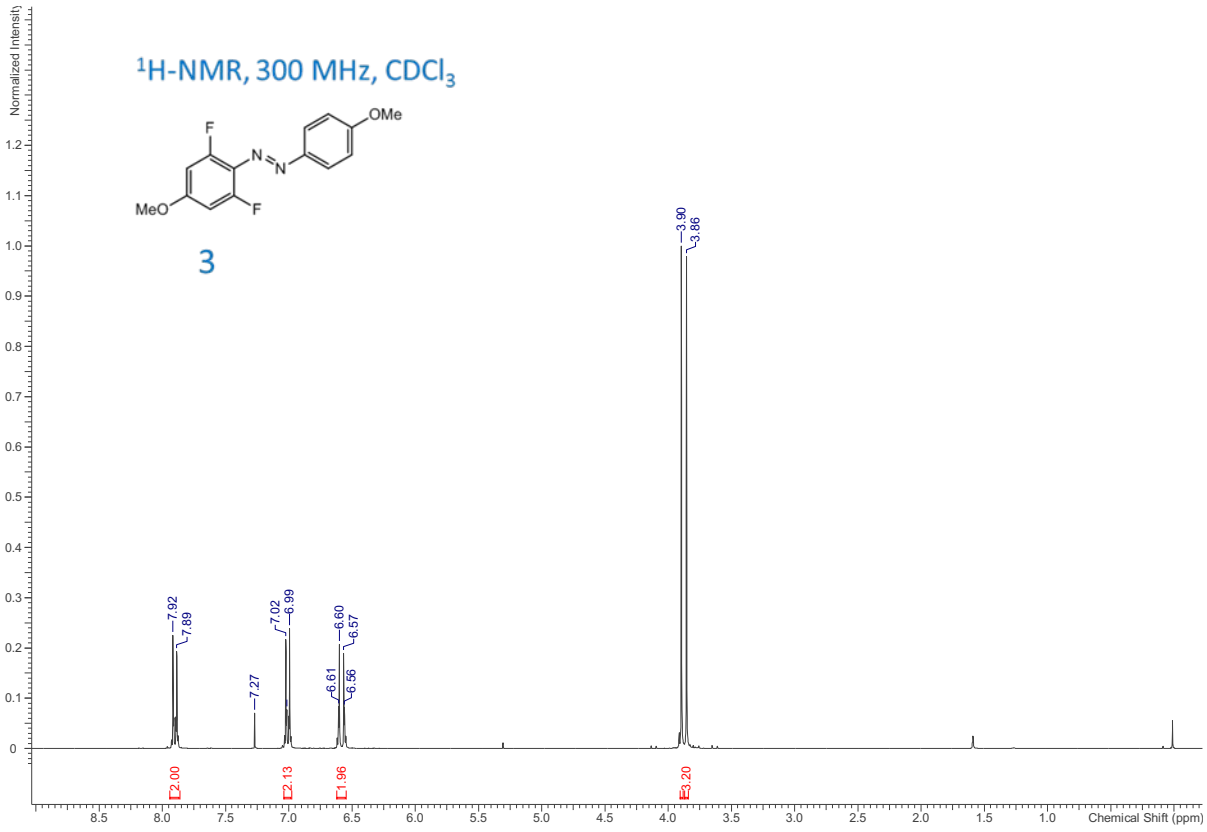
1H-NMR, 300 MHz, CDCl3
F
N
N
OMe
MeO
F
3
Normalized Intensity
7.92
7.89
7.27
7.02
6.99
6.61
6.60
6.57
6.56
3.90
3.86
I2.00
I2.13
I1.96
I3.20
Chemical Shift (ppm)

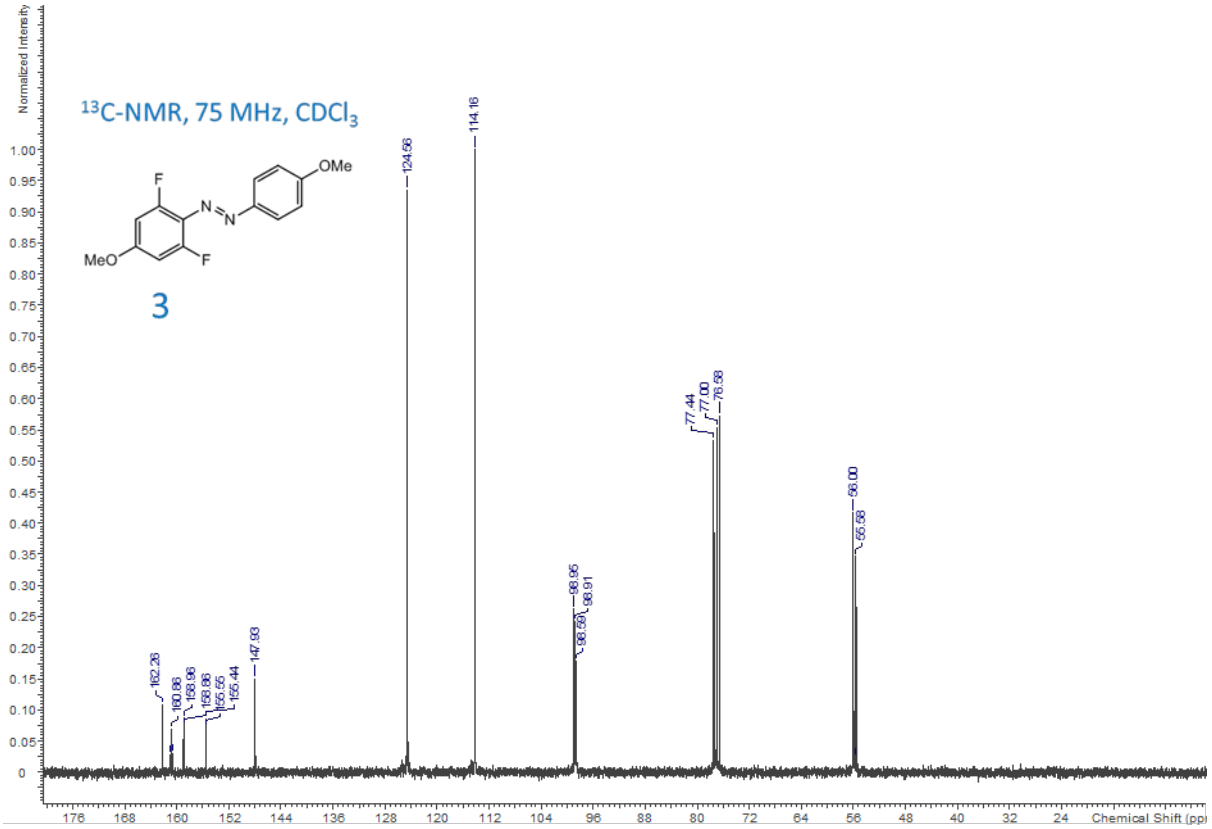
13C-NMR, 75 MHz, CDCl3
F
N
N
OMe
MeO
F
3
Normalized Intensity
162.26
160.86
158.96
156.86
155.55
155.44
147.93
124.56
114.16
98.95
98.69
98.91
77.44
77.00
76.68
56.00
55.98
Chemical Shift (ppm)

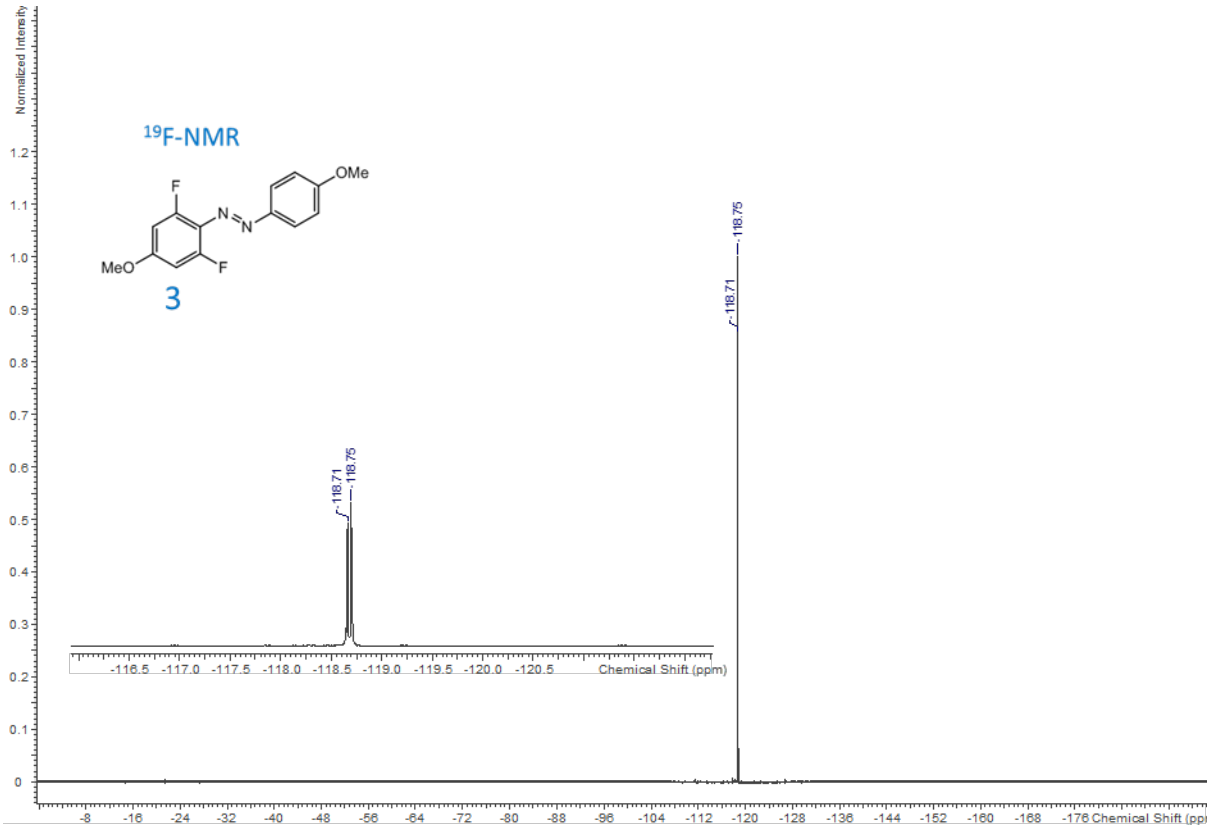
19F-NMR
OMe
F
N
N
MeO
F
3
-118.71
-118.75
Chemical Shift (ppm)

Compound **4**

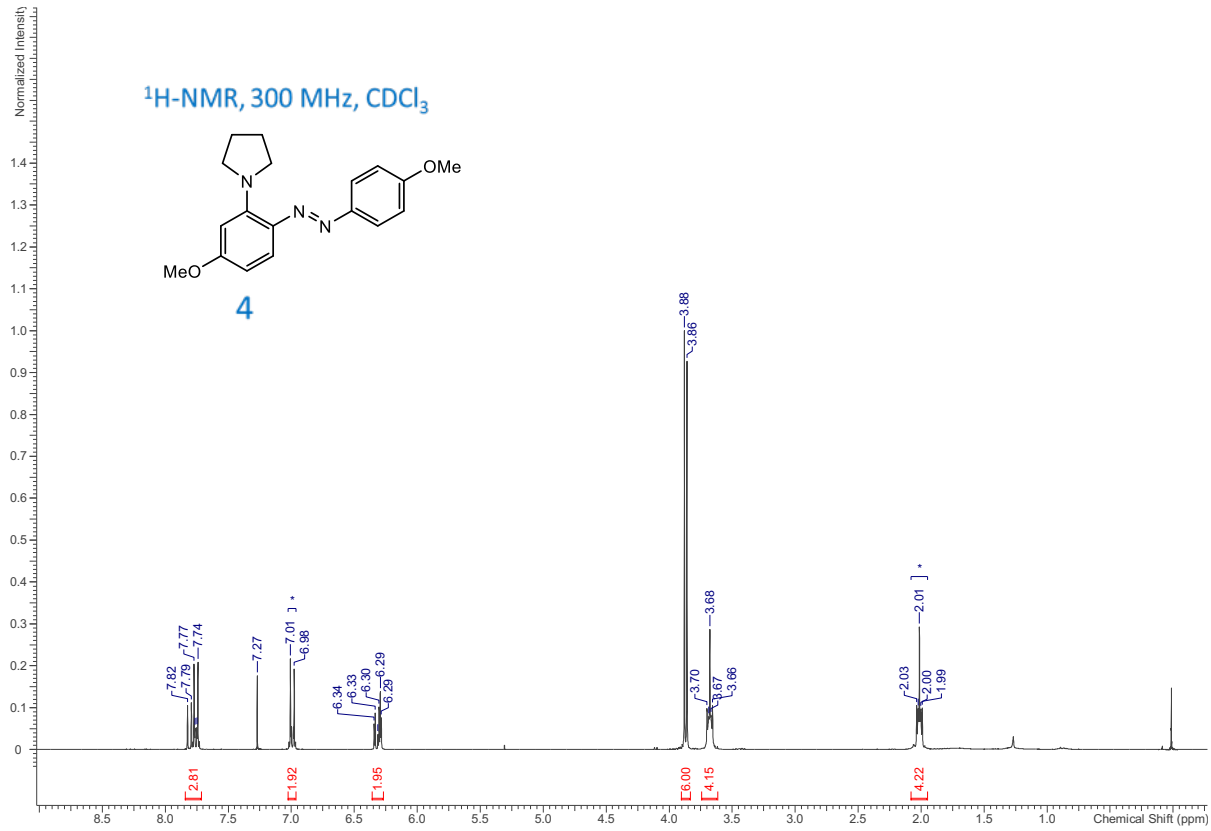
1H-NMR, 300 MHz, CDCl3
N
OMe
N
N
MeO
4
Chemical Shift (ppm)

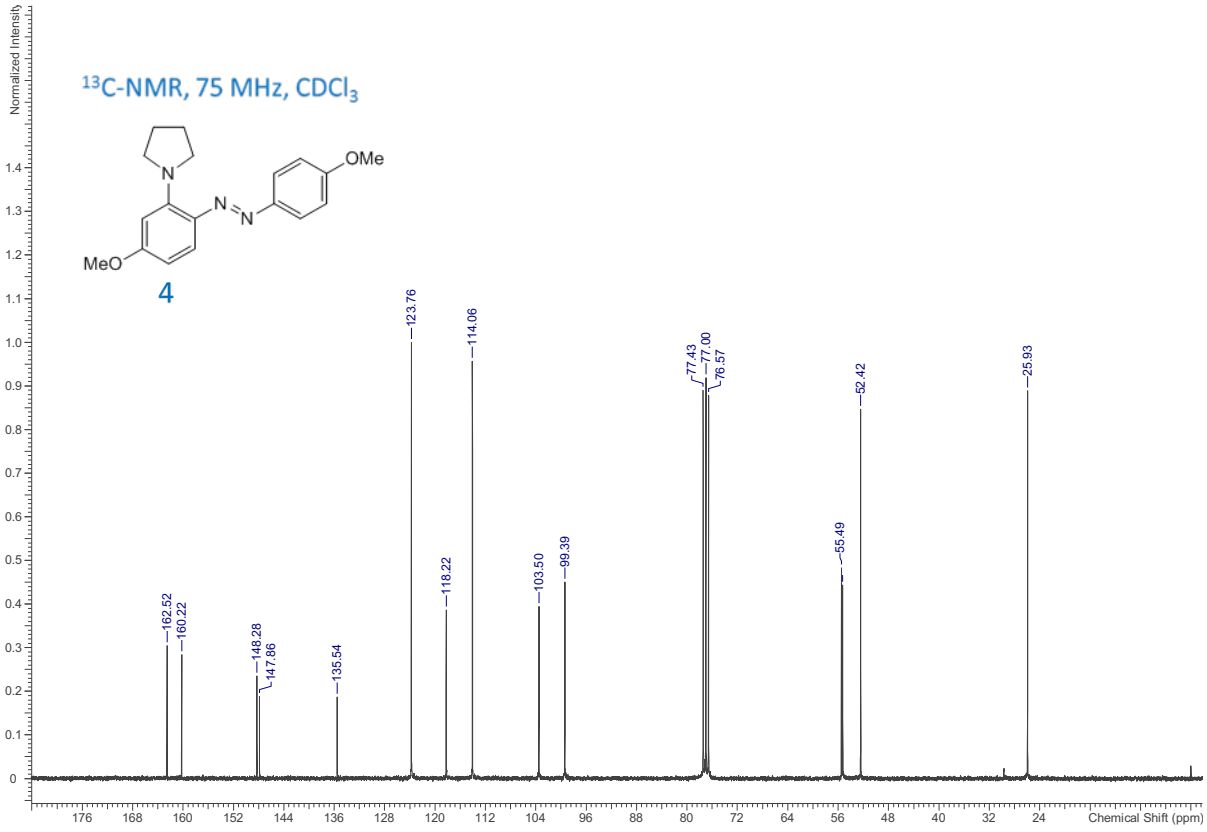
13C-NMR, 75 MHz, CDCl3
OMe
MeO
4
Normalized Intensity
123.76
114.06
118.22
103.50
99.39
77.43
77.00
76.57
52.42
55.49
25.93
162.52
160.22
148.28
147.86
135.54
Chemical Shift (ppm)

Compound **5**

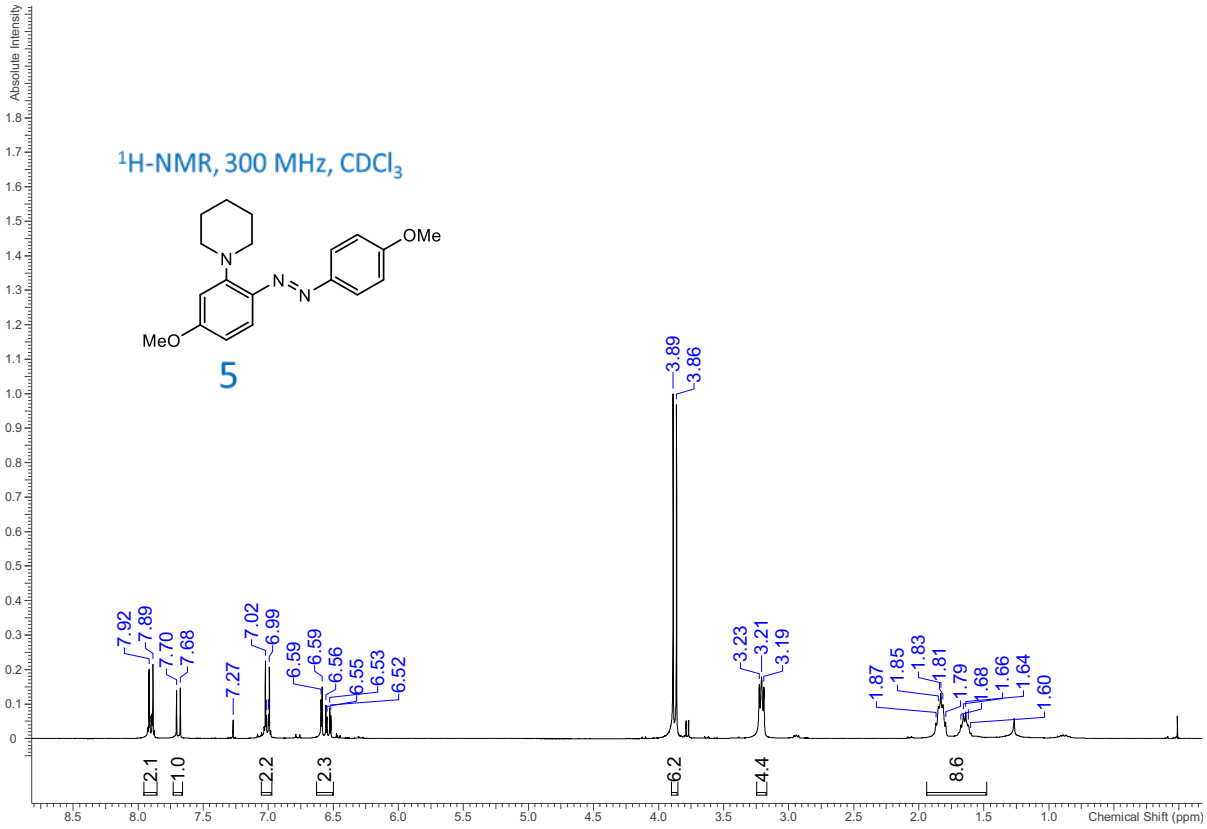
1H-NMR, 300 MHz, CDCl3
OMe
MeO
5
Absolute Intensity
3.89
3.86
7.92
7.89
7.70
7.68
7.27
7.02
6.99
6.59
6.59
6.56
6.55
6.53
6.52
3.23
3.21
3.19
1.87
1.85
1.83
1.81
1.79
1.68
1.66
1.64
1.60
2.1
1.0
2.2
2.3
6.2
4.4
8.6
Chemical Shift (ppm)

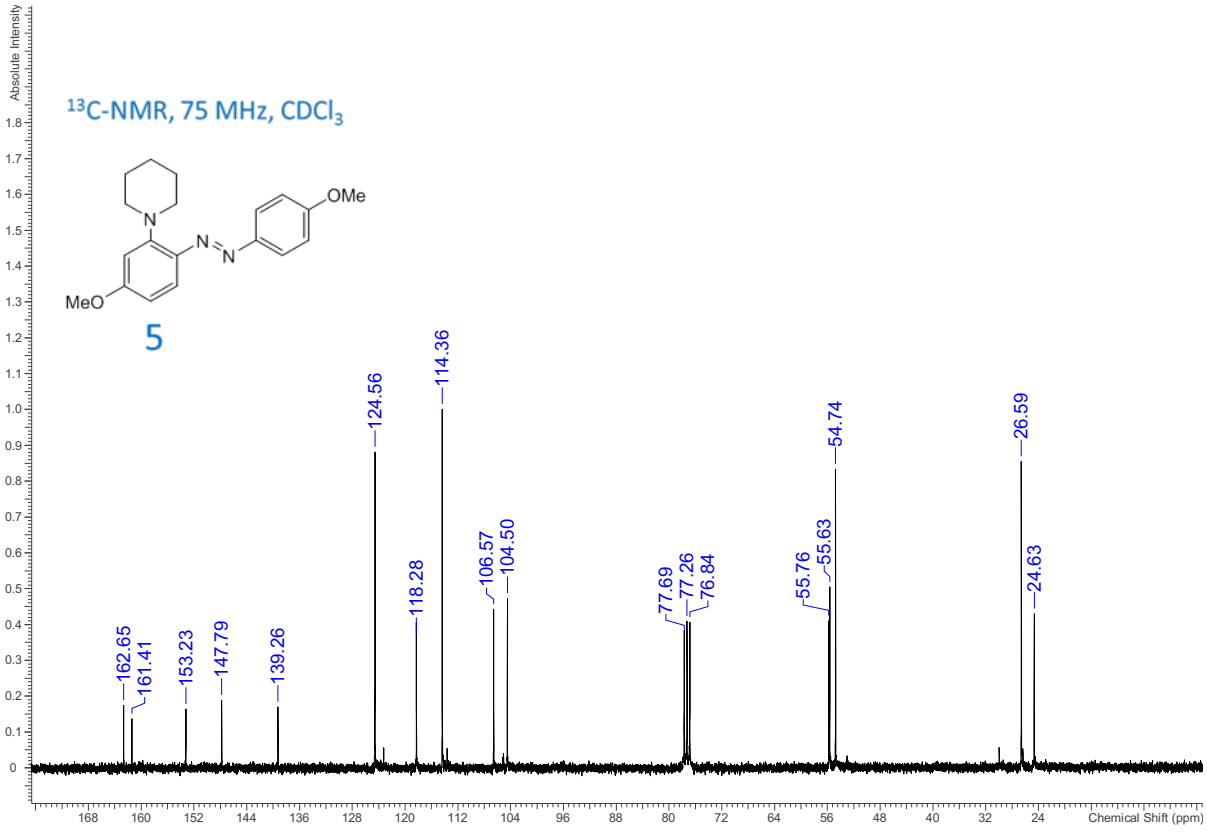
13C-NMR, 75 MHz, CDCl3
OMe
N
N
N
MeO
5
Absolute Intensity
162.65
161.41
153.23
147.79
139.26
124.56
118.28
114.36
106.57
104.50
77.69
77.26
76.84
55.76
55.63
54.74
26.59
24.63
Chemical Shift (ppm)

Compound **6**

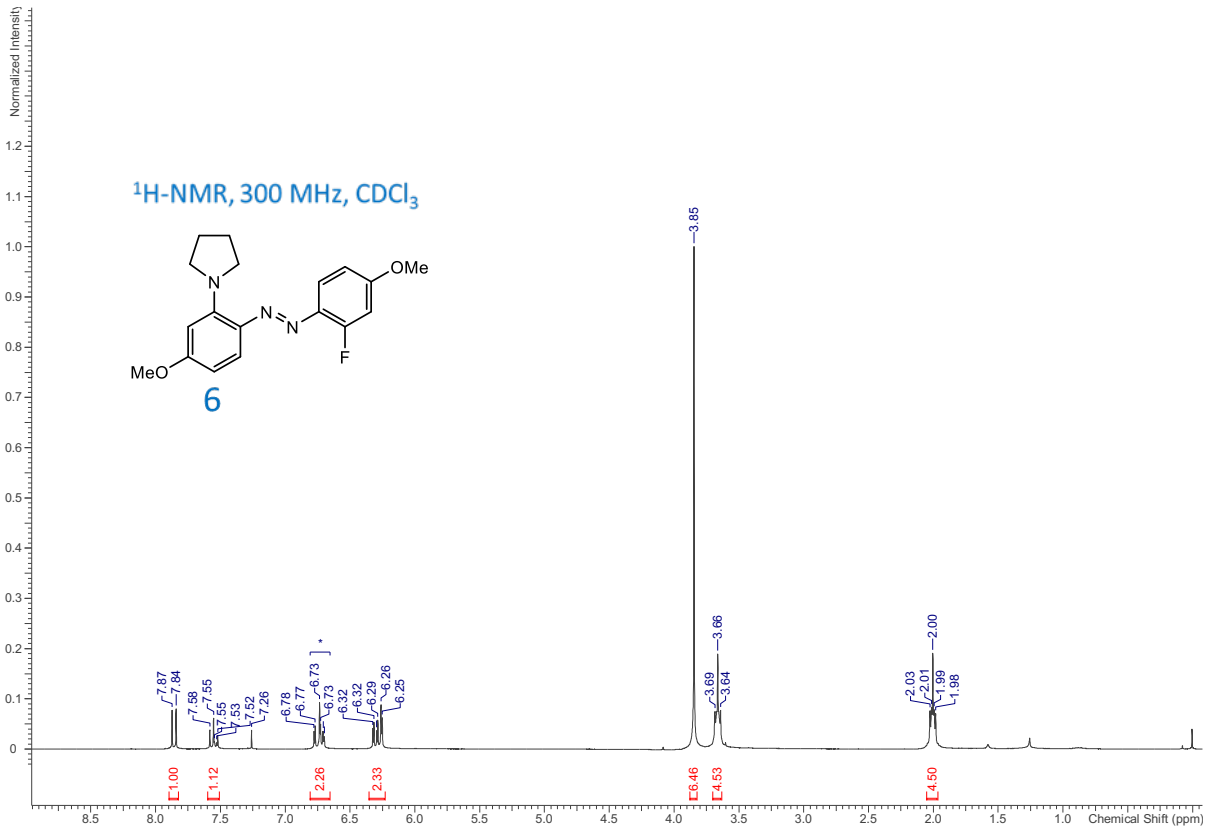
1H-NMR, 300 MHz, CDCl3
OMe
N
N
N
F
MeO
6
Normalized Intensity
3.85
3.66
3.69
3.64
2.00
2.03
2.01
1.99
1.98
7.87
7.84
7.58
7.55
7.55
7.53
7.52
7.26
6.78
6.77
6.73
6.73
6.32
6.29
6.26
6.25
1.00
1.12
2.26
2.33
6.46
4.53
4.50
Chemical Shift (ppm)

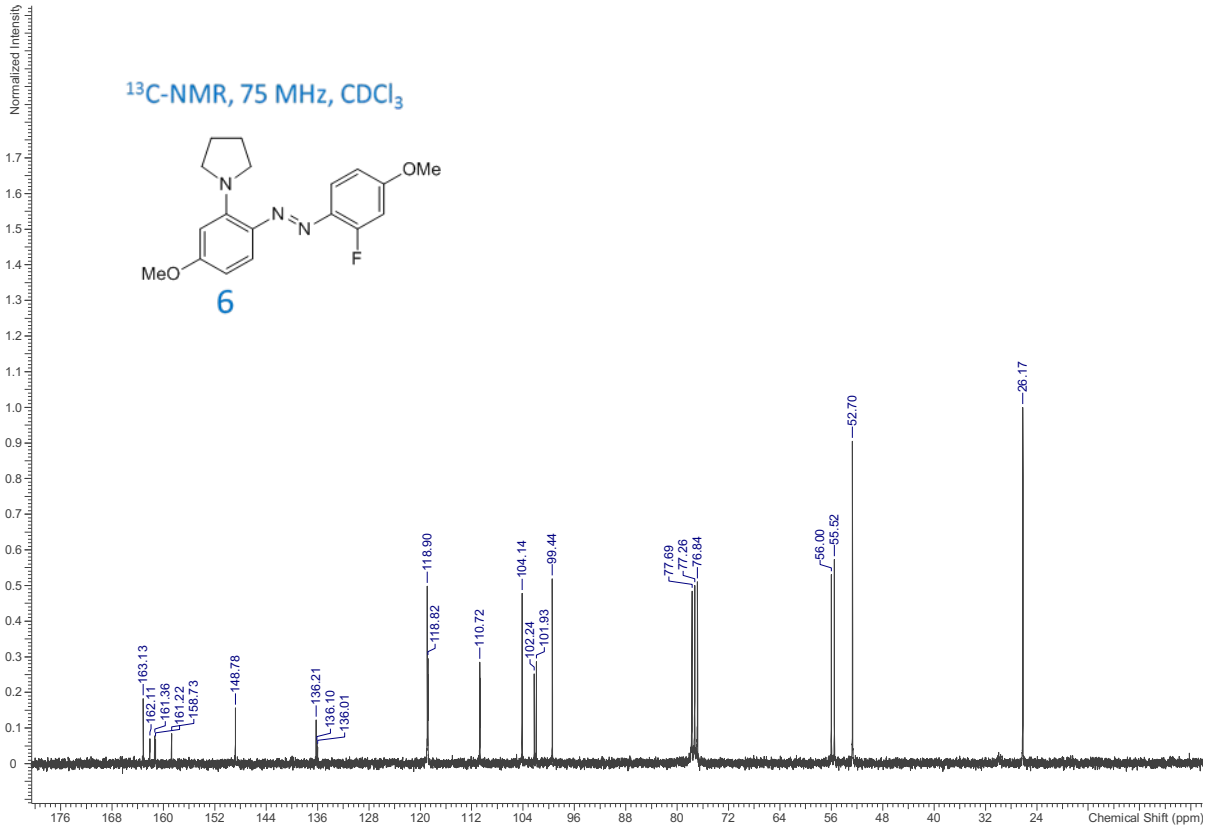
13C-NMR, 75 MHz, CDCl3
OMe
N
N
N
MeO
F
6
Normalized Intensity
163.13
162.11
161.36
161.22
158.73
148.78
136.21
136.10
136.01
118.90
118.82
110.72
104.14
102.24
101.93
99.44
77.69
77.26
76.84
56.00
55.52
52.70
26.17
Chemical Shift (ppm)

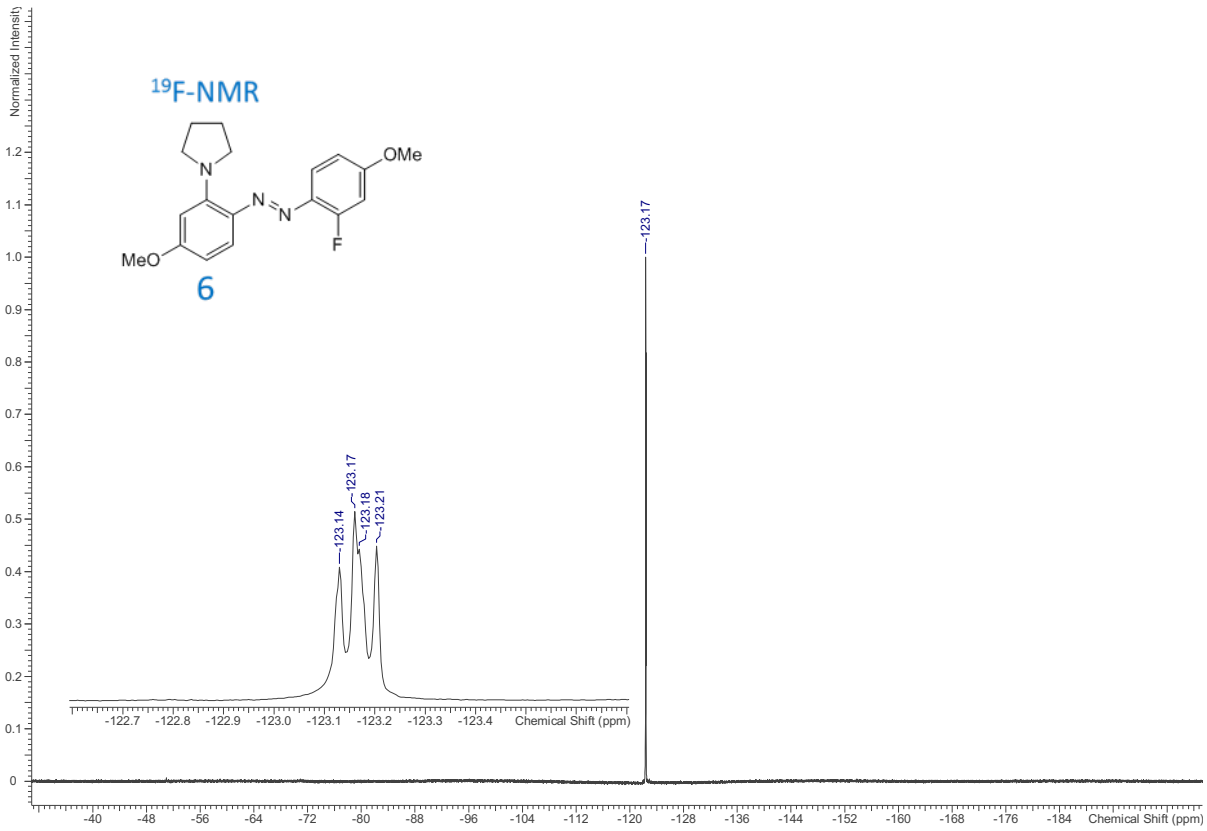
19F-NMR
OMe
N
N
N
MeO
F
6
Normalized Intensity
123.17
123.14
123.17
123.18
123.21
Chemical Shift (ppm)
Chemical Shift (ppm)

Compound **7**

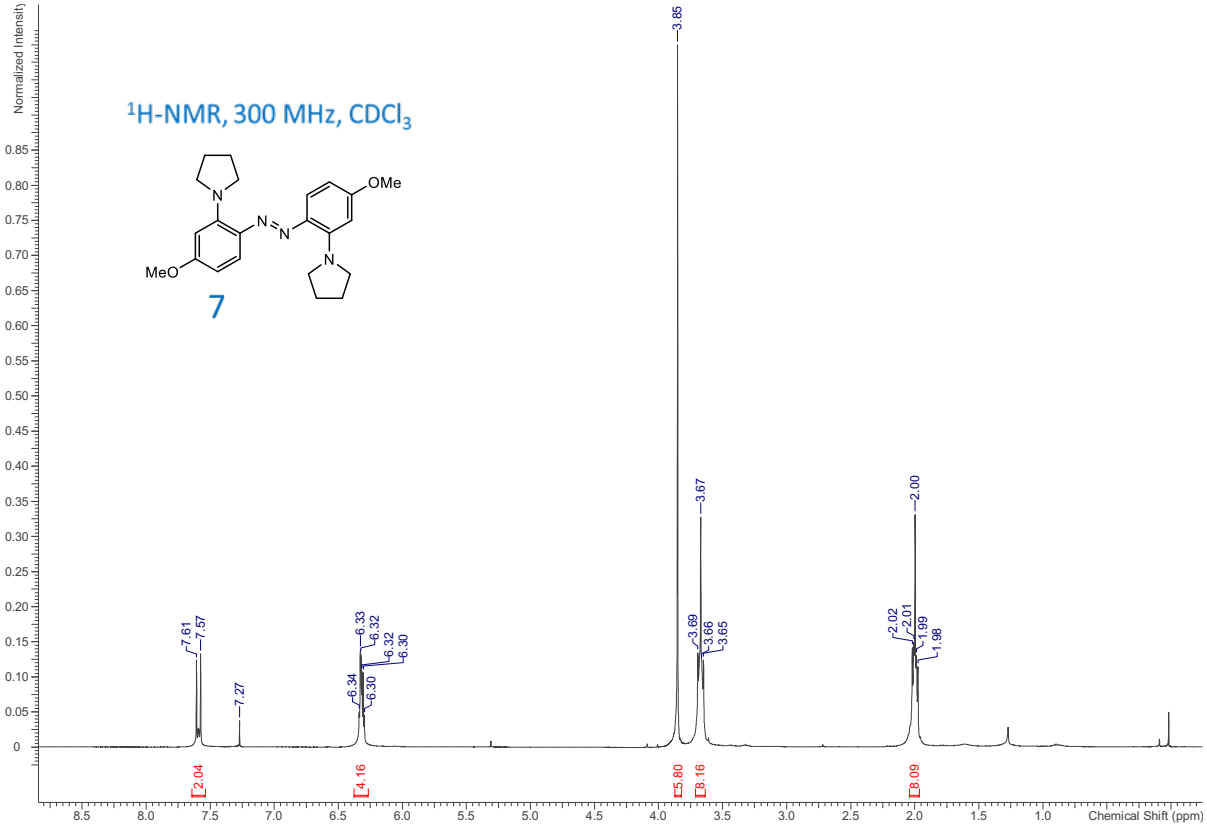
^{1}H-NMR, 300 MHz, $CDCl_3$
OMe
MeO
7
Normalized Intensity
Chemical Shift (ppm)
3.85
3.67
2.00
7.61
7.57
7.27
6.33
6.32
6.32
6.30
6.34
6.30
3.69
3.66
3.65
2.02
2.01
1.99
1.98
2.04
4.16
5.80
3.16
8.09

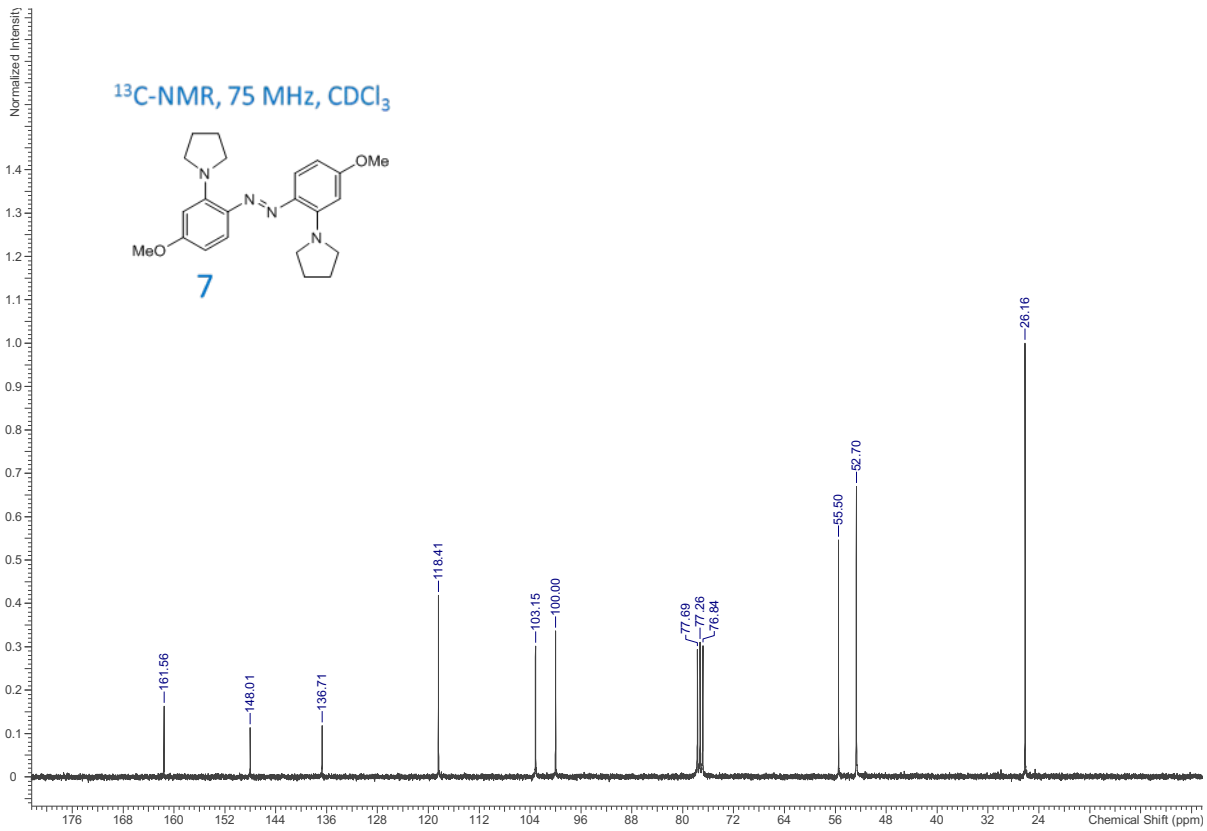
^{13}C-NMR, 75 MHz, $CDCl_3$
OMe
MeO
7
Normalized Intensity
Chemical Shift (ppm)
161.56
148.01
136.71
118.41
103.15
100.00
77.69
77.26
76.84
55.50
52.70
26.16

Compound **8**

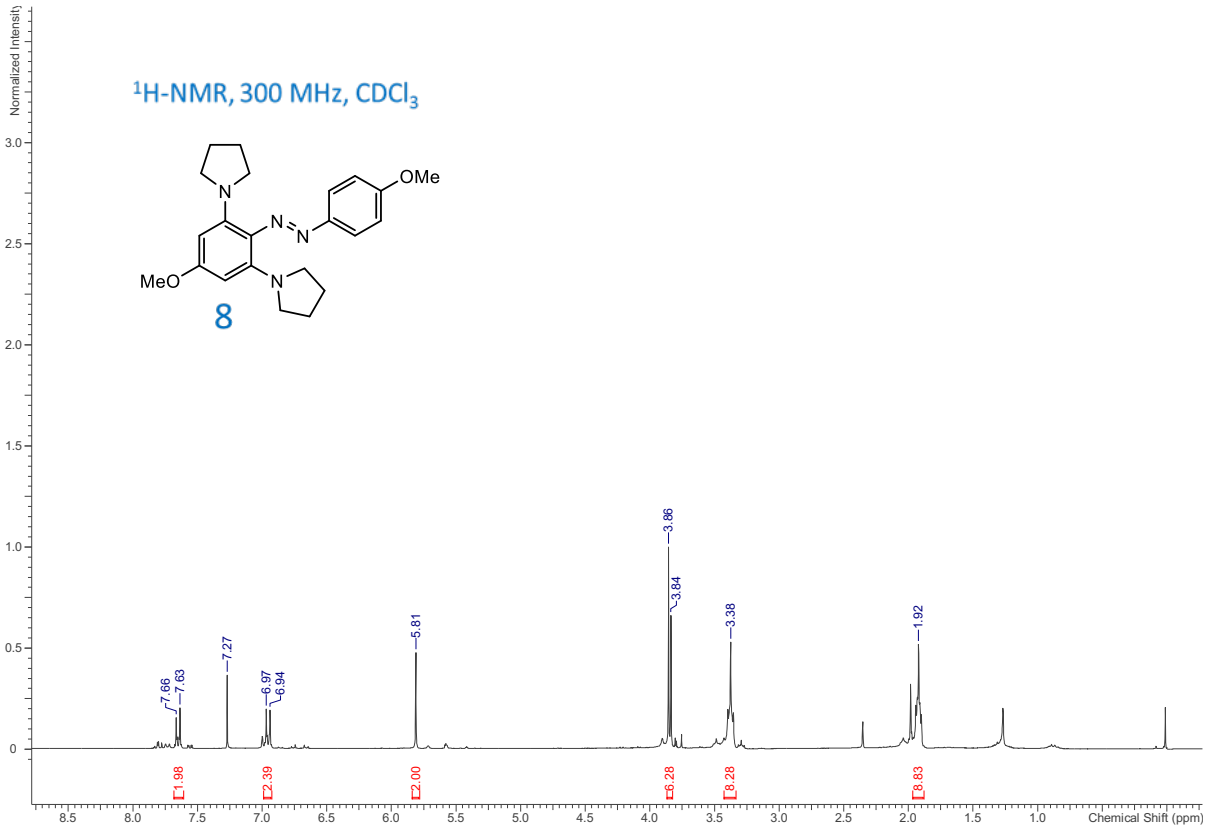
Normalized Intensity
^{1}H-NMR, 300 MHz, $CDCl_3$
OMe
MeO
N
N
N
8
7.66
7.63
7.27
6.97
6.94
5.81
3.86
3.84
3.38
1.92
1.98
2.39
2.00
6.28
8.28
8.83
Chemical Shift (ppm)

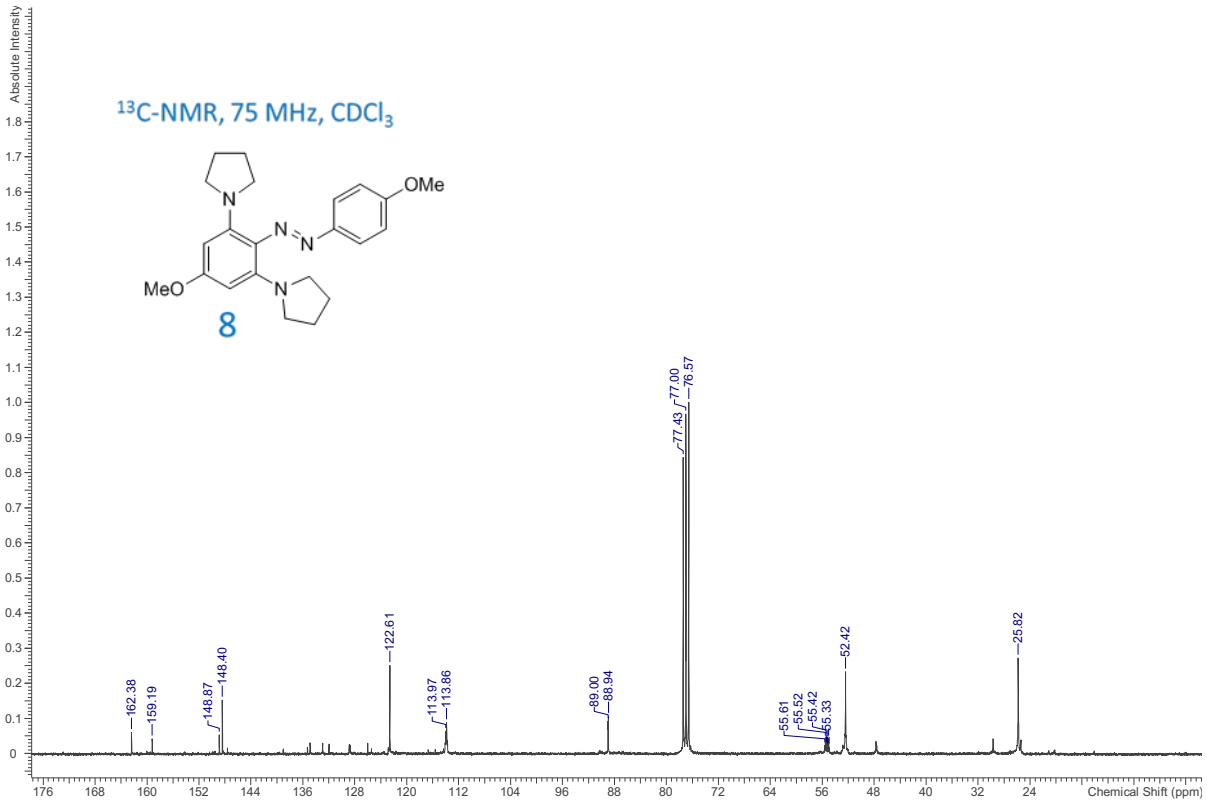
Absolute Intensity
^{13}C-NMR, 75 MHz, $CDCl_3$
OMe
MeO
N
N
N
8
162.38
159.19
148.87
148.40
122.61
113.97
113.86
89.00
88.94
77.43
77.00
76.57
55.61
55.52
55.42
55.33
52.42
25.82
Chemical Shift (ppm)

Compound **9**

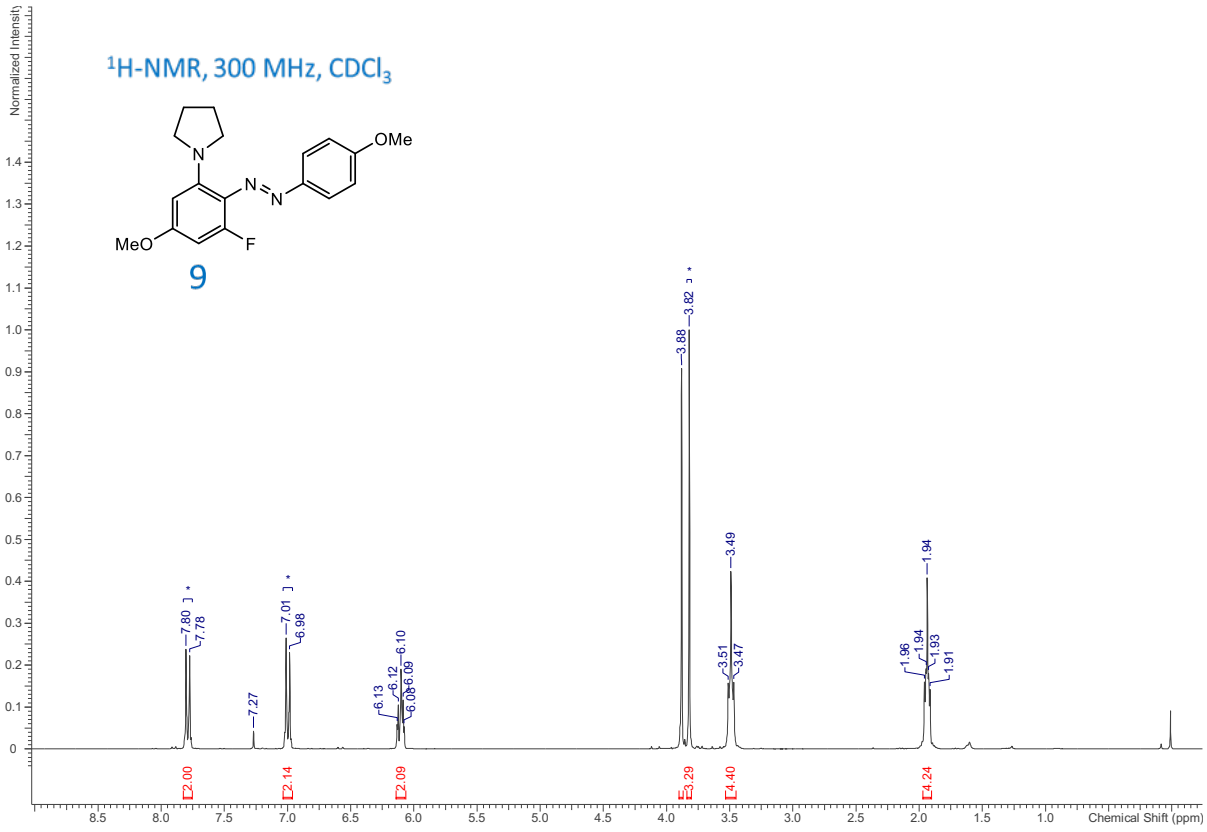
^{1}H-NMR, 300 MHz, $CDCl_3$
OMe
N
N
N
MeO
F
9
Normalized Intensity
Chemical Shift (ppm)

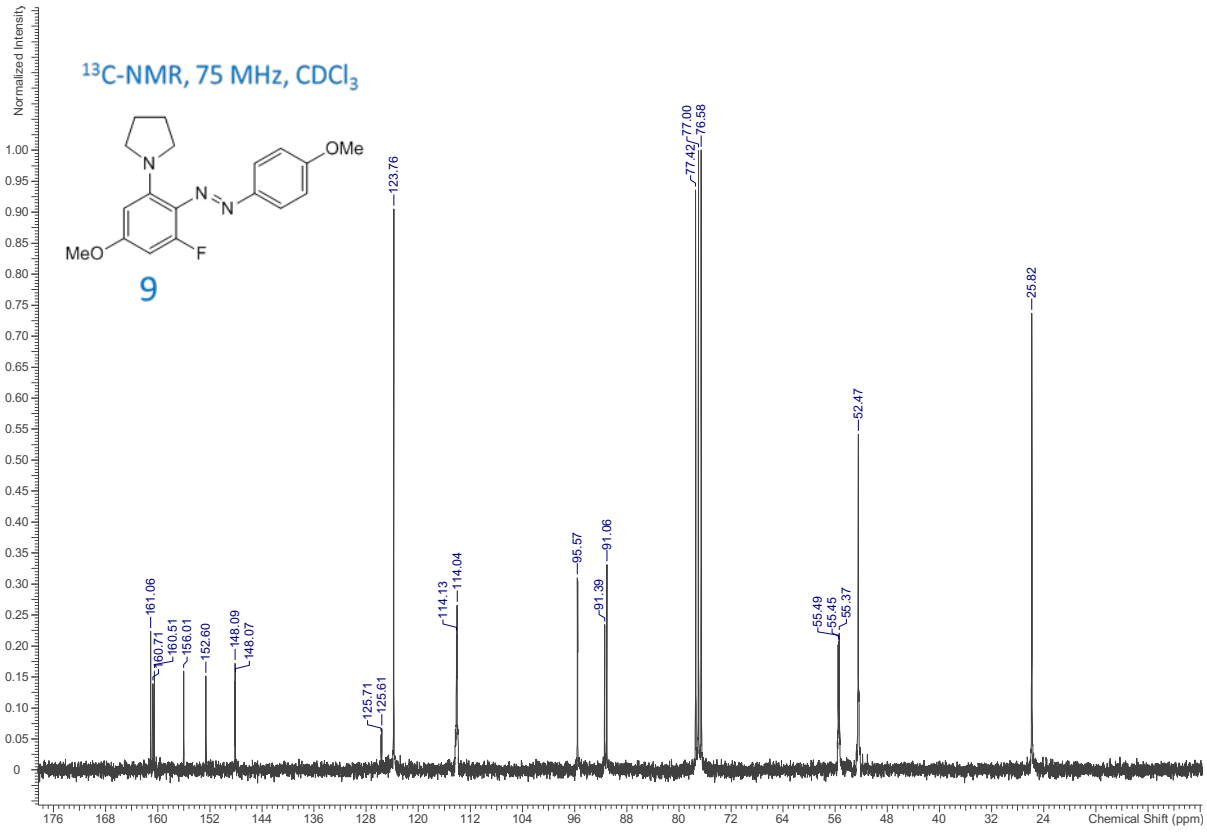
^{13}C-NMR, 75 MHz, $CDCl_3$
OMe
N
N
N
MeO
F
9
Normalized Intensity
Chemical Shift (ppm)

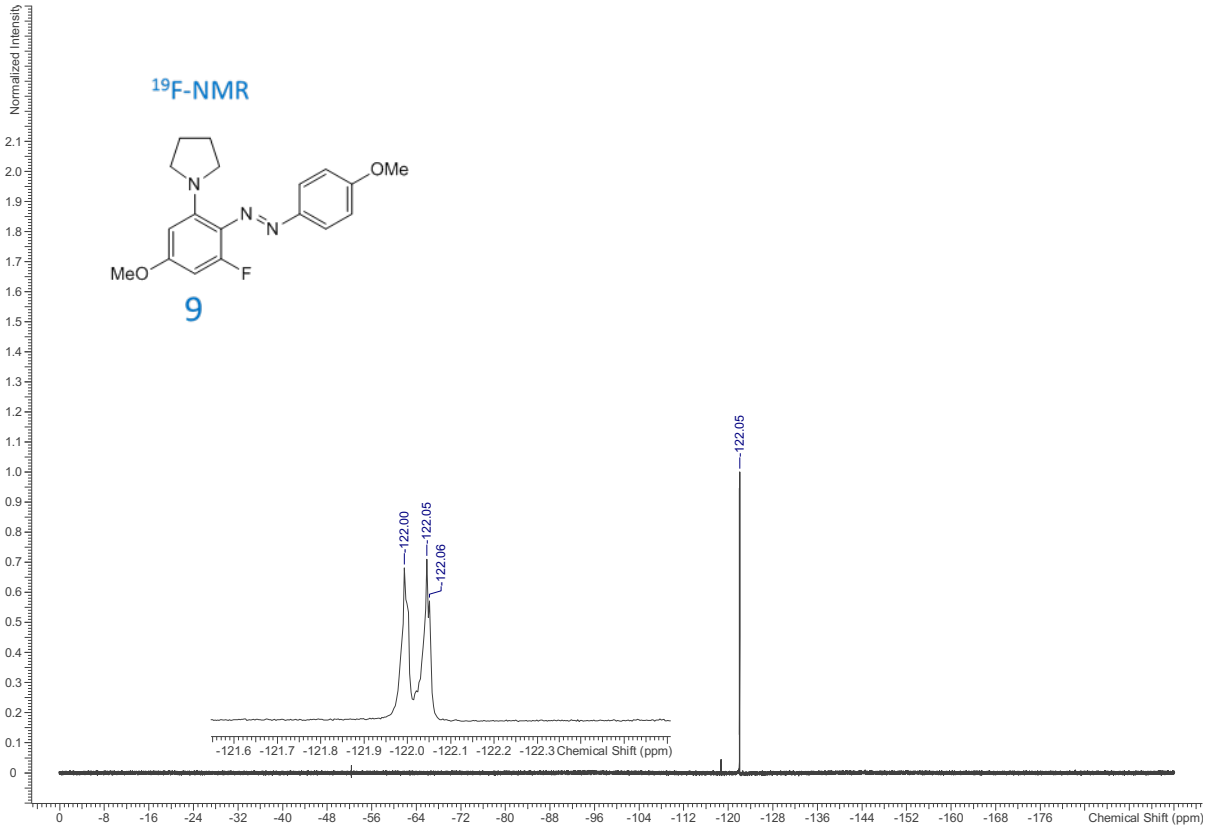
19F-NMR
OMe
N
N
N
MeO
F
9
Normalized Intensity
-122.00
-122.05
-122.06
-122.05
-121.6 -121.7 -121.8 -121.9 -122.0 -122.1 -122.2 -122.3 Chemical Shift (ppm)
0 -8 -16 -24 -32 -40 -48 -56 -64 -72 -80 -88 -96 -104 -112 -120 -128 -136 -144 -152 -160 -168 -176 Chemical Shift (ppm)

6. Mass spectra

Compound **1**

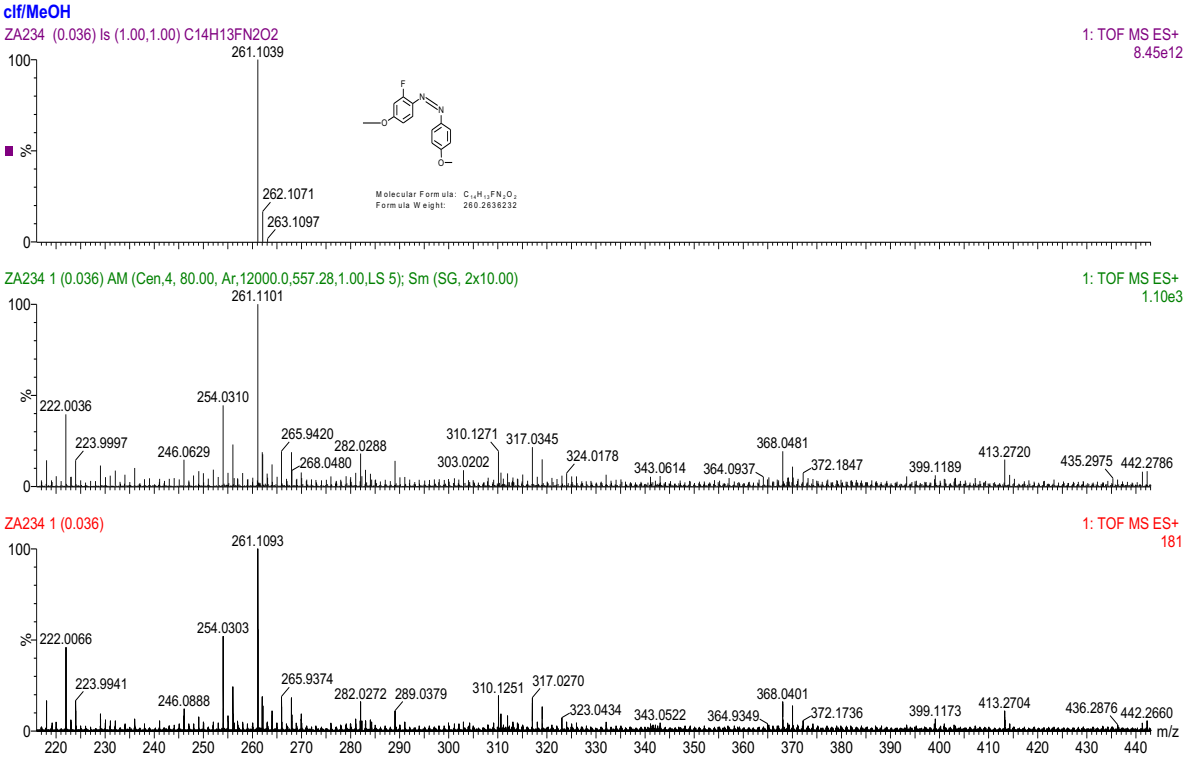

Compound **2**

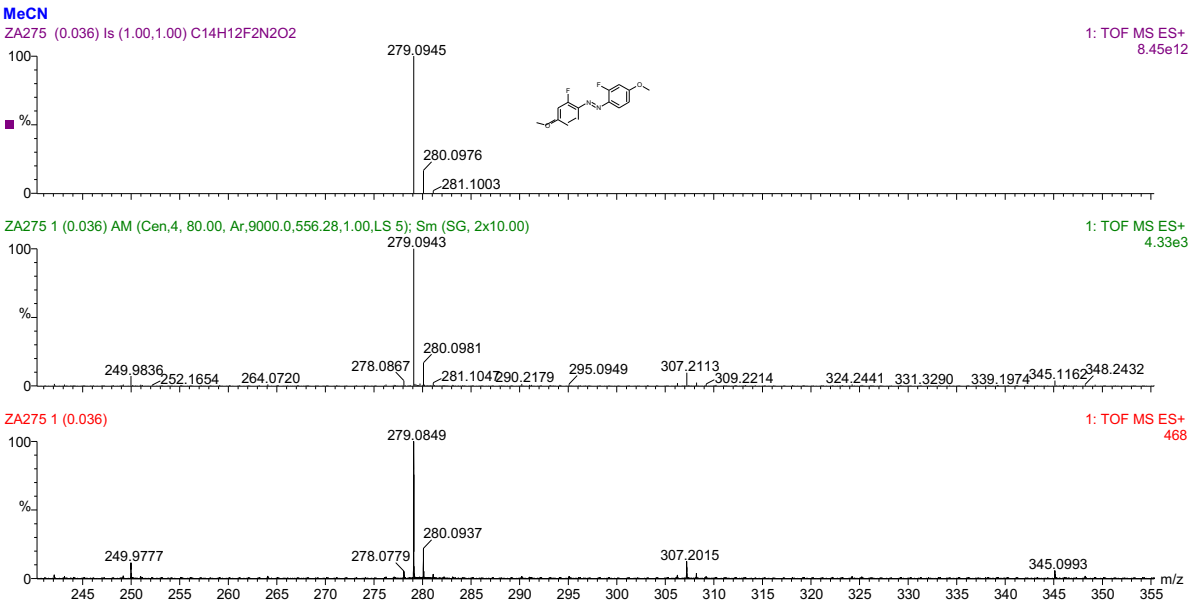

Compound **3**

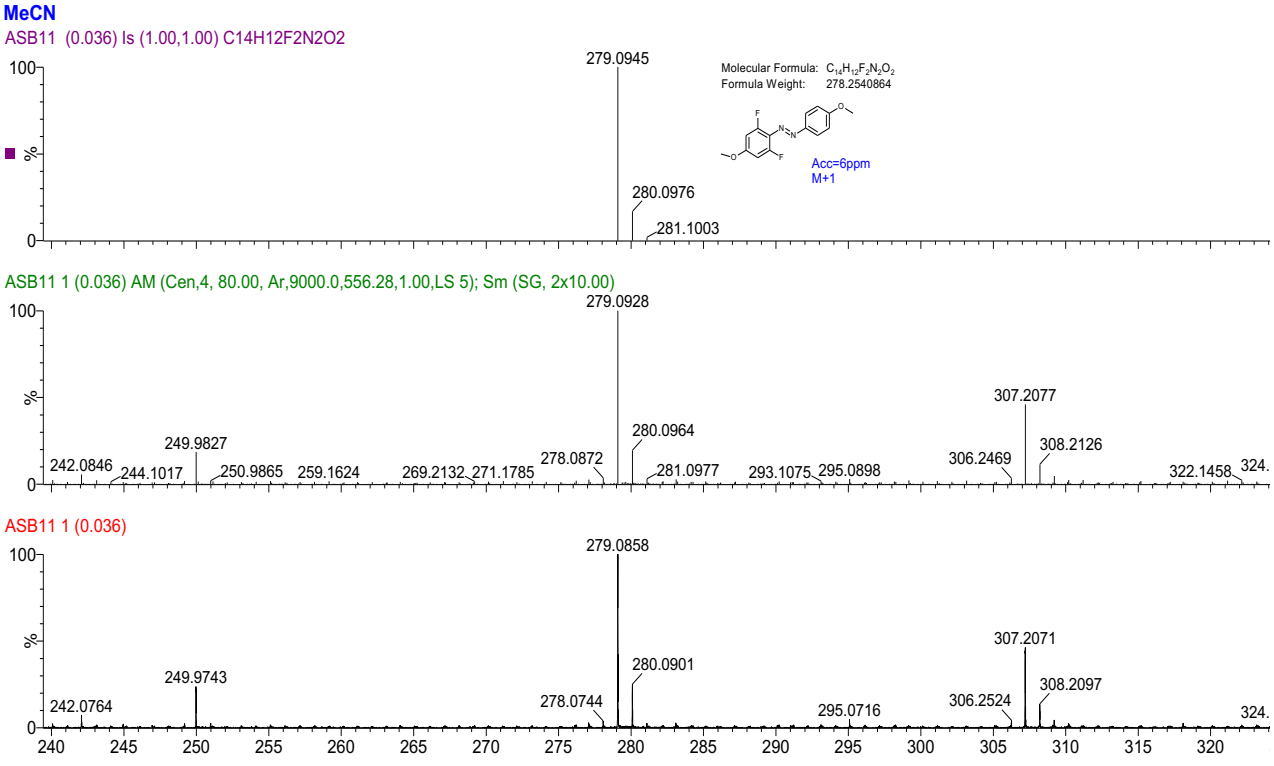

Compound **4**

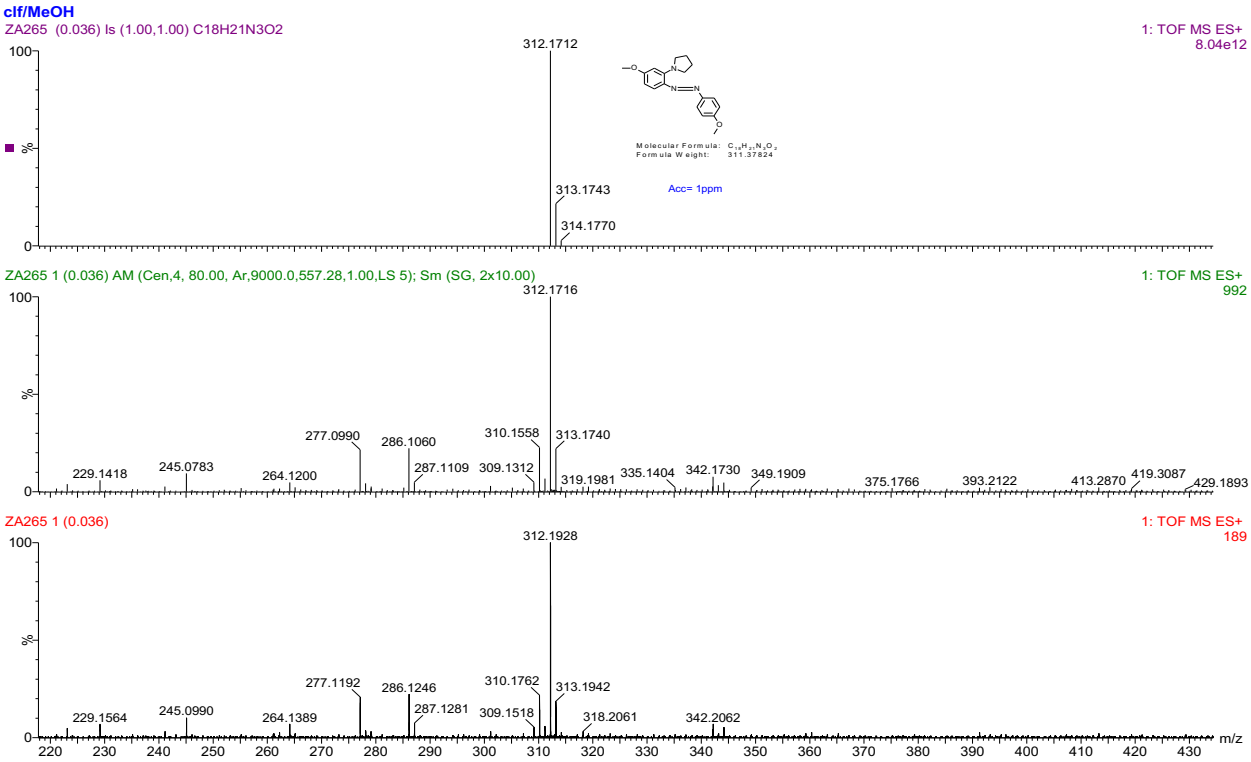

Compound **5**

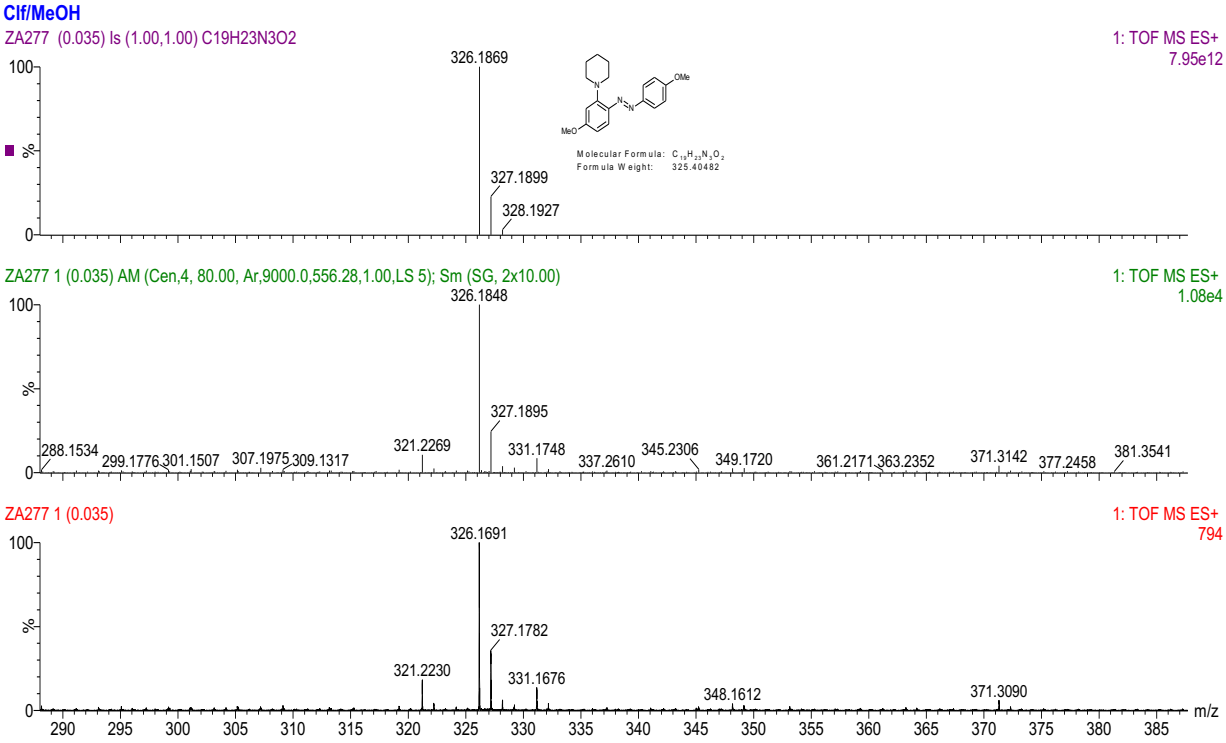

Compound **6**

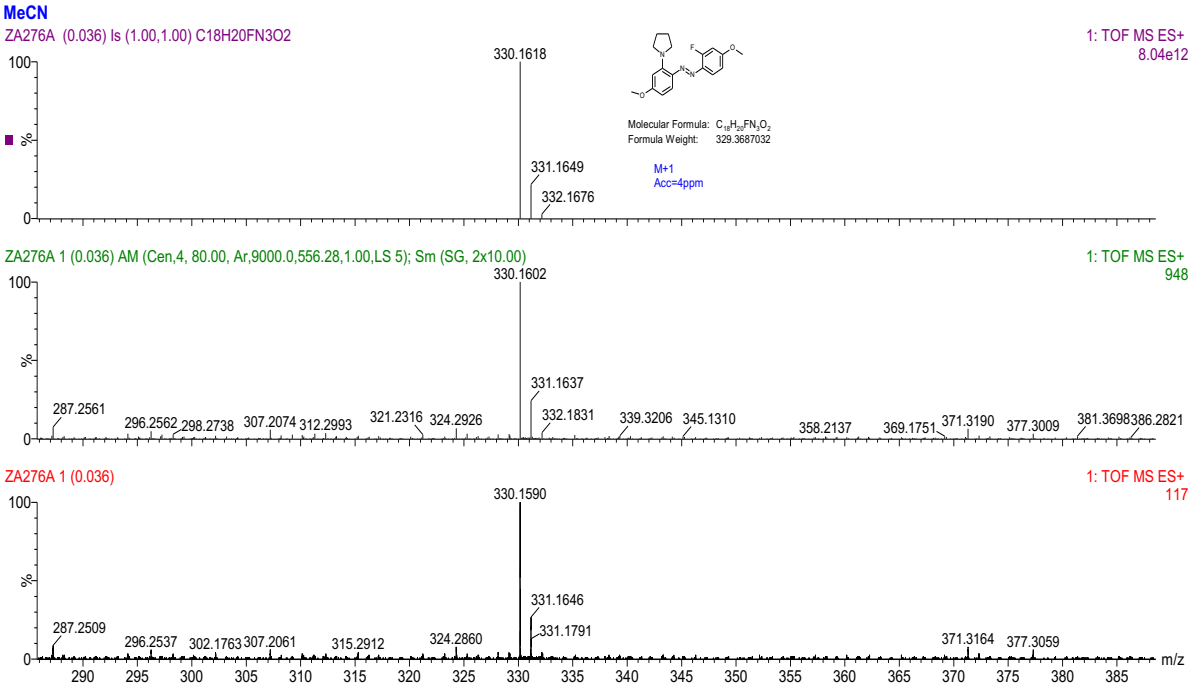

Compound **7**

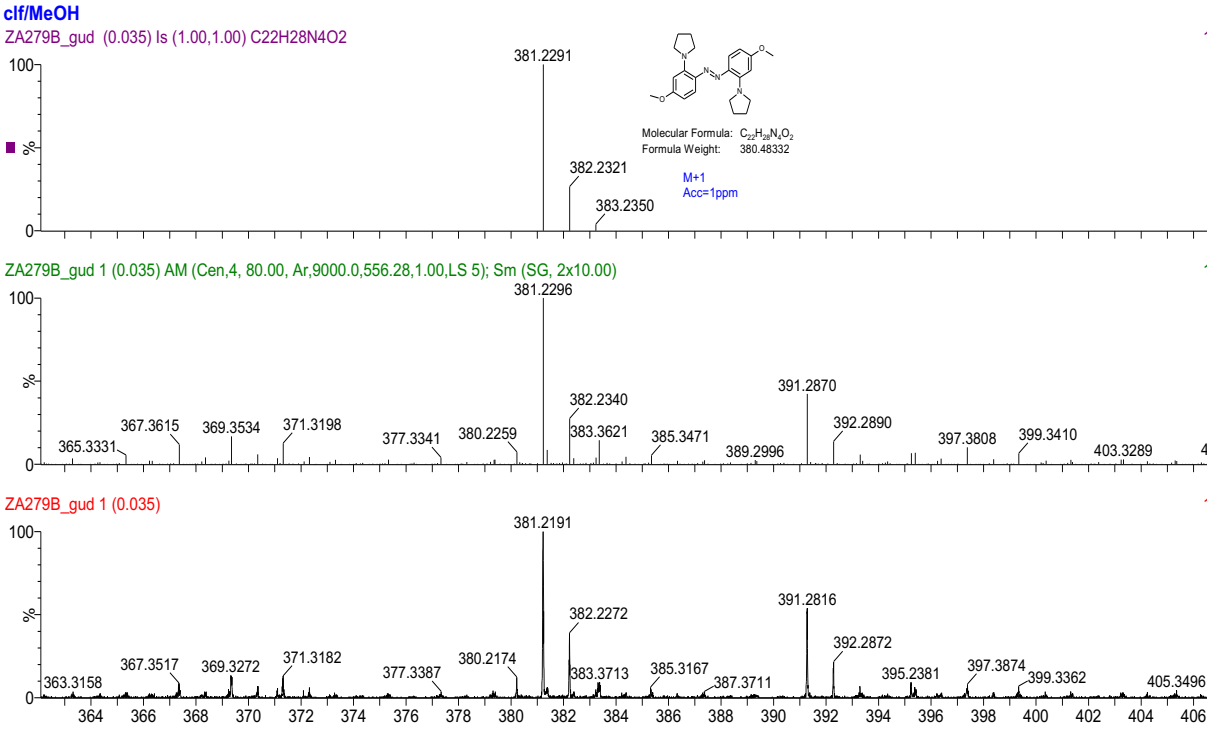

Compound **8**

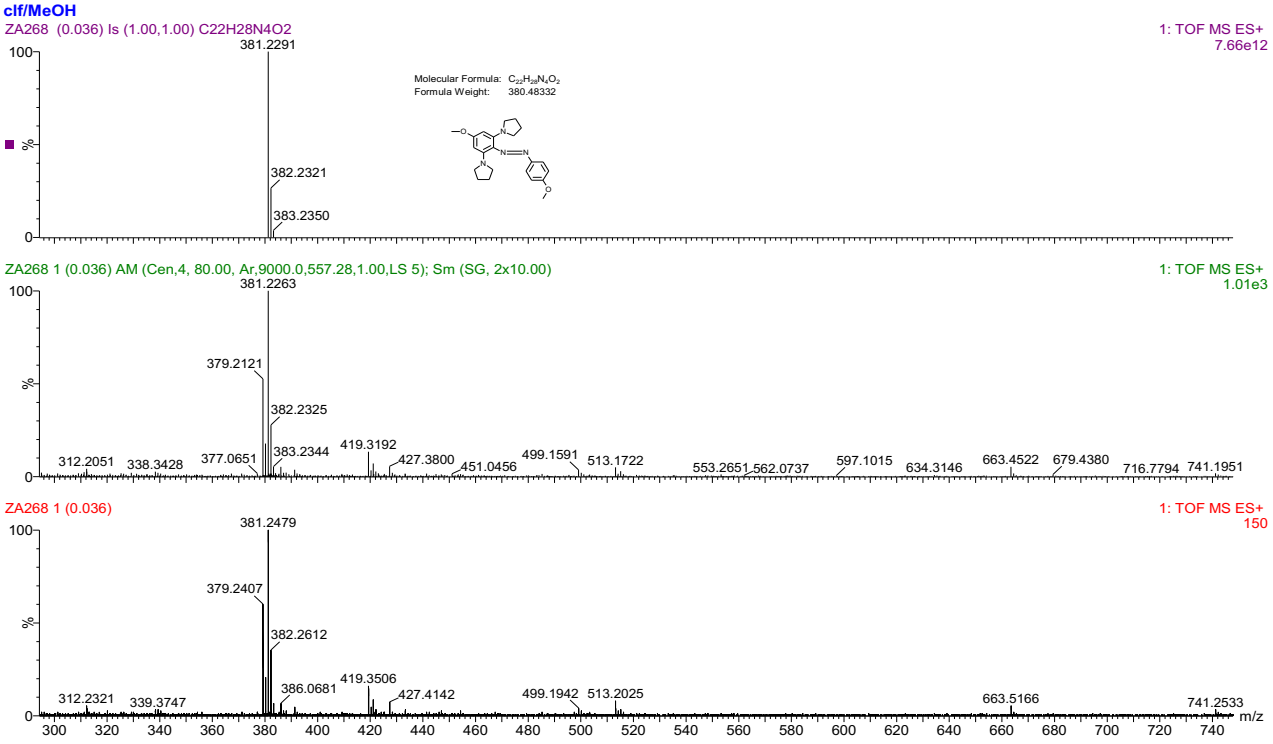

Compound **9**

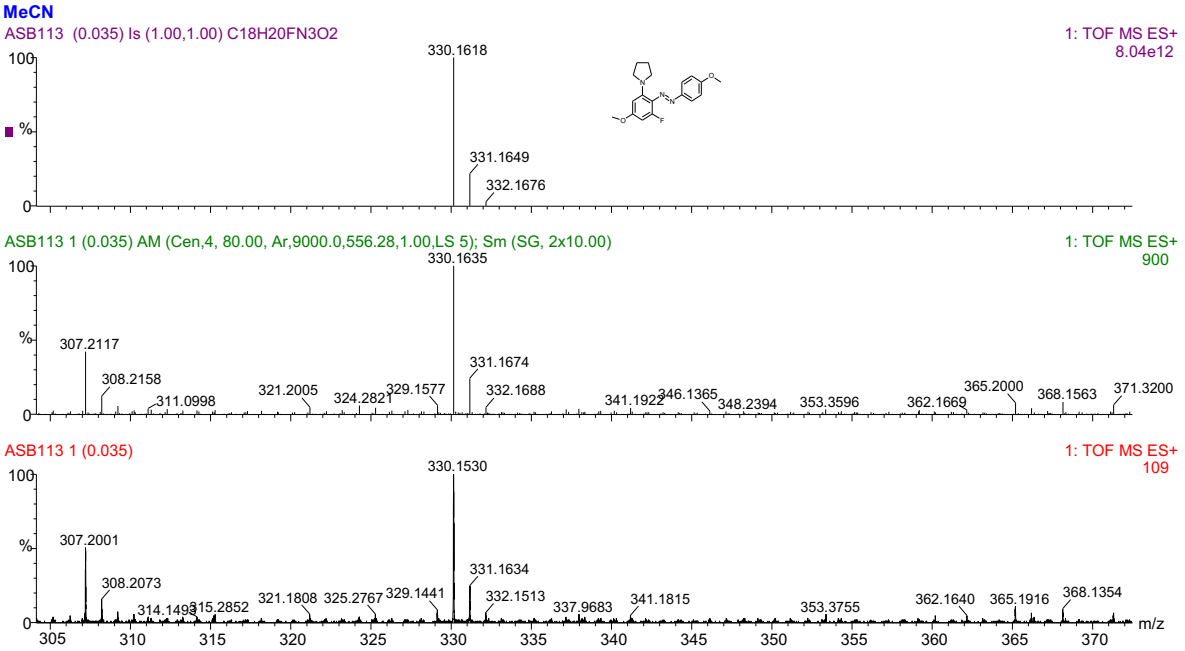

7. Photoisomerization studies

UV–visible absorption spectra were recorded using 1 cm quartz cuvettes on an Agilent Cary 60 spectrophotometer equipped with an Ocean Optics qpod 2e Peltier-thermostated cell holder (temperature accuracy ± 0.1 °C). Photoexcitation experiments were performed using a Prior Lumen 1600 light source with multiple choices for narrow-band LEDs at different wavelengths. The photoexcitation wavelength was chosen for each compound near an absorption maximum. The power density was about 250 mW cm^{-2} and the samples were illuminated for 30–90 seconds until a photostationary state was reached. All measurements were done in spectrophotometric grade acetonitrile.

The measurements for compounds **1**–**3**, **5** and **9** were carried out at 50, 60 and 70 ºC due to their *cis*-lifetimes being impractically long for a direct measurement at 25 ºC. UV–visible spectra were measured with time intervals chosen such that around ten points are measured while the absorbance is seen to return by at least 80 % towards the dark-adapted value after photoexcitation. The *cis*-isomer decay was studied by observing the absorbance at a wavelength chosen on the long-wavelength edge (about 80 % of maximum absorption) of

the longest-wavelength absorption peak clearly visible in the *trans*-rich absorption spectrum.

Single exponential fits where performed to determine the *cis* lifetime at each temperature. The fitting equation[2] was $-(A_{inf} - A_0)\times e^{-kt} + A_{inf}$, where A_{inf} is the absorbance after infinite time i.e. absorbance in dark, A_0 is the absorbance at the beginning of *cis* decay, i.e. absorbance at photostationary state, k it the *cis*-decay rate constant and t is time. The parameters A_{inf}, A_0 and k were used as free parameters in the fits. The *cis*-lifetimes were then calculated as $\tau = \frac{1}{k}$ where necessary. The natural logarithm of k was calculated at each temperature and plotted as a function of inverse temperature. From these Arrhenius plots, the *cis*-lifetimes at 25 ºC were extracted by linear fitting and extrapolation. Error estimates were extracted from the Arrhenius plots by calculating the maximum and minimum values for the lifetimes given by the error limits of the Arrhenius plot extrapolation. The error estimate given is the maximum minus minimum divided by two.

Compounds **4**, **6** and **7** were measured at 25 ºC. The values reported for compounds **6** and **7** were measured at the same time of the year. Repetition of the measurement after a few months for **6** and **7** gave notably shorter lifetime values from same synthetic batch. This variation might be due to moisture and a varying humidity level at different times of the year. Compounds **4** and **7** were studied by continuously monitoring the absorbance at a selected wavelength and compound **6** by measuring the absorption spectrum with chosen intervals. A Single exponential function mathematically identical to the one used for compounds **1**–**3, 5** and **9** was used to determine the cis lifetimes directly from these measurements and the standard error given by fitting was used for the error estimate.

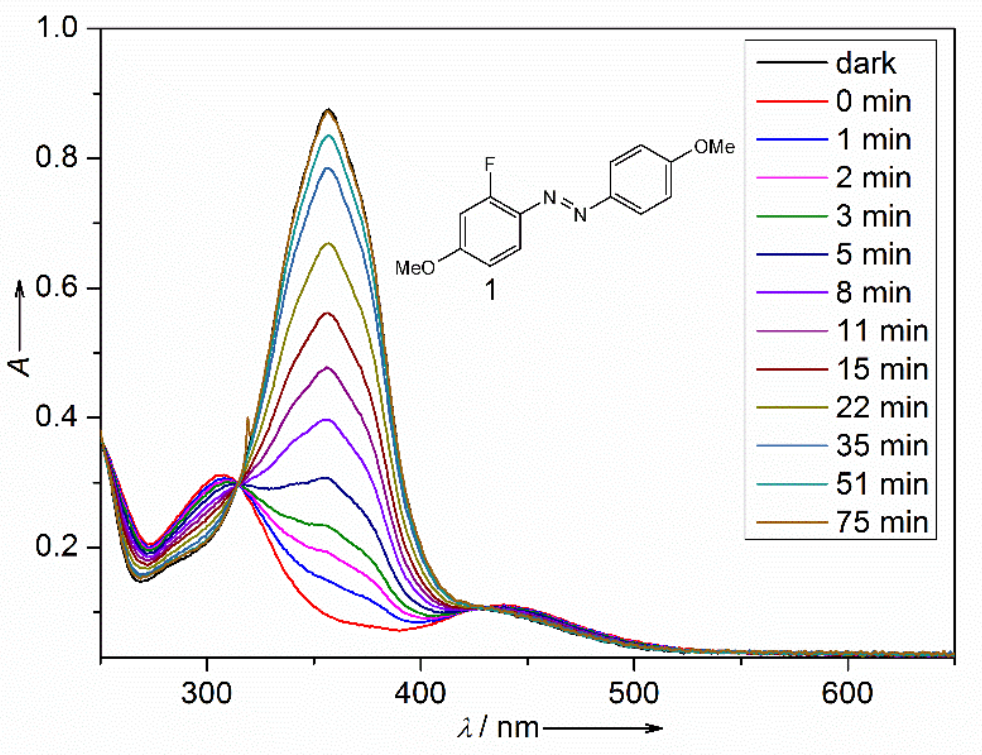

Figure S21. Thermal *cis*-to-*trans* isomerization of compound **1** at 70°C.

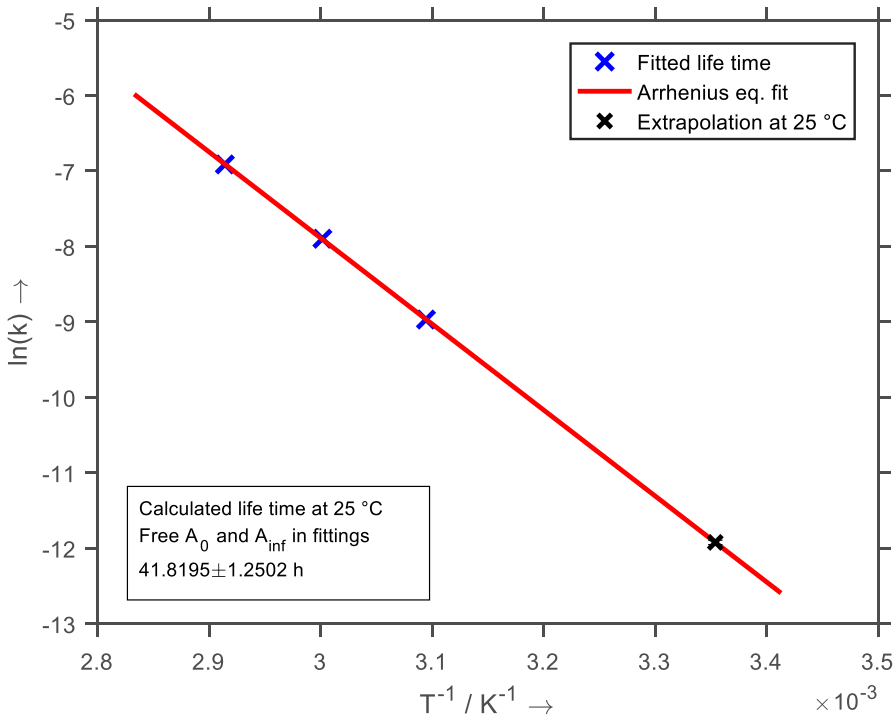

Figure S22. Arrhenius plot of compound **1**.

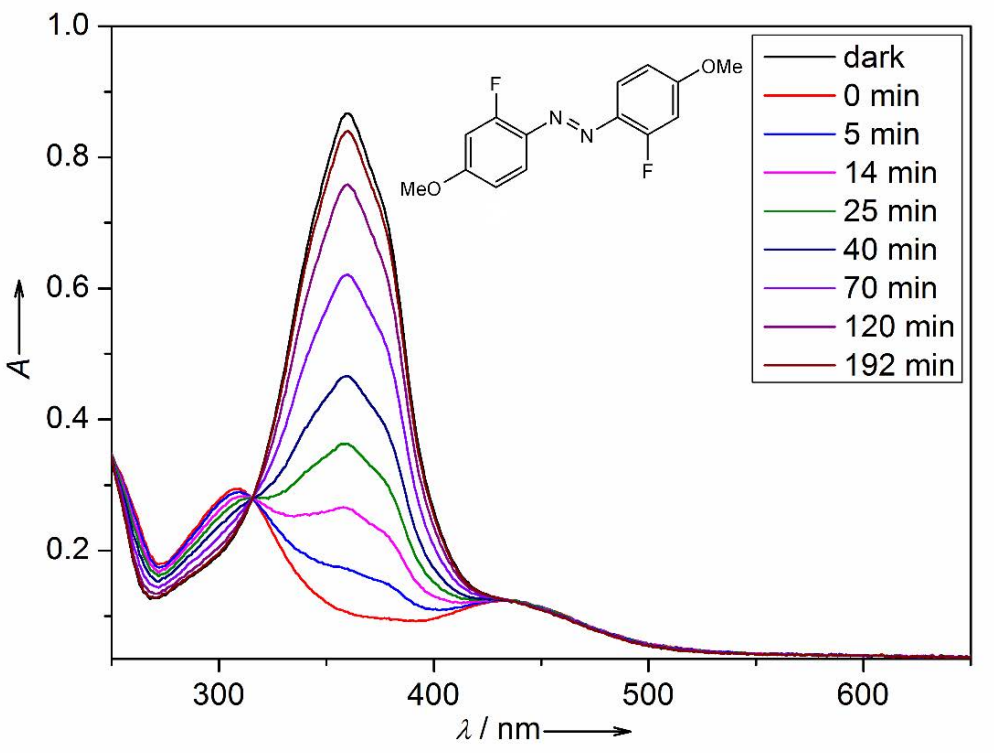

Figure S23. Thermal *cis*-to-*trans* isomerization of compound **2** at 70°C.

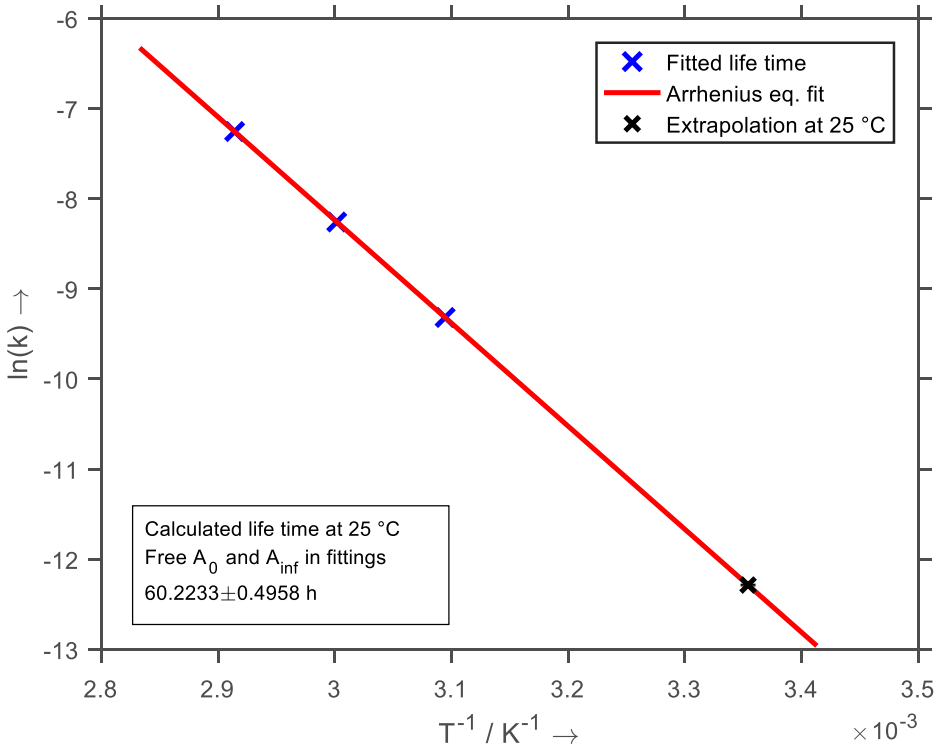

Figure S24. Arrhenius plot of compound **2**.

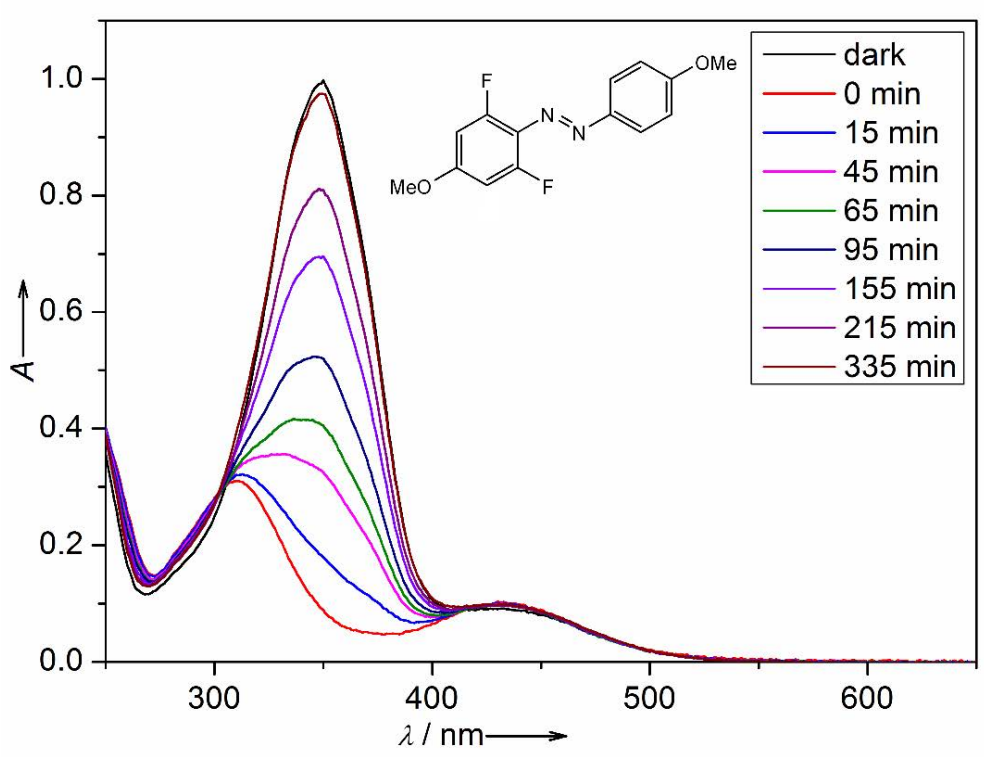

Figure S25. Thermal *cis*-to-*trans* isomerization of compound **3** at 60°C.

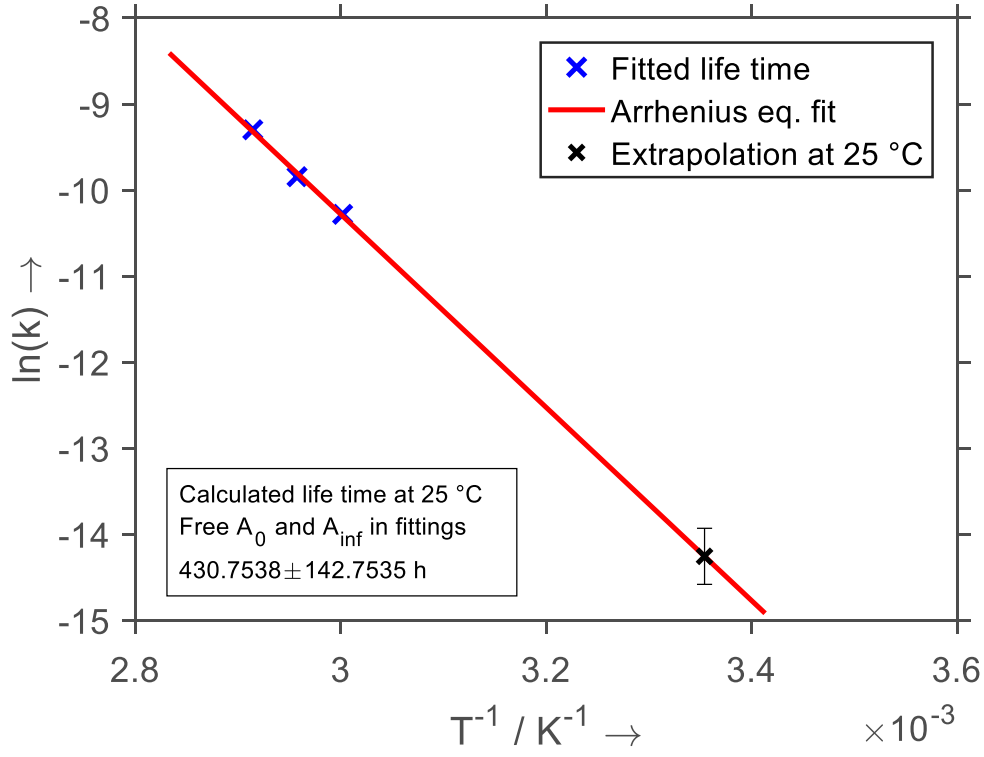

Figure S26. Arrhenius plot of compound **3**.

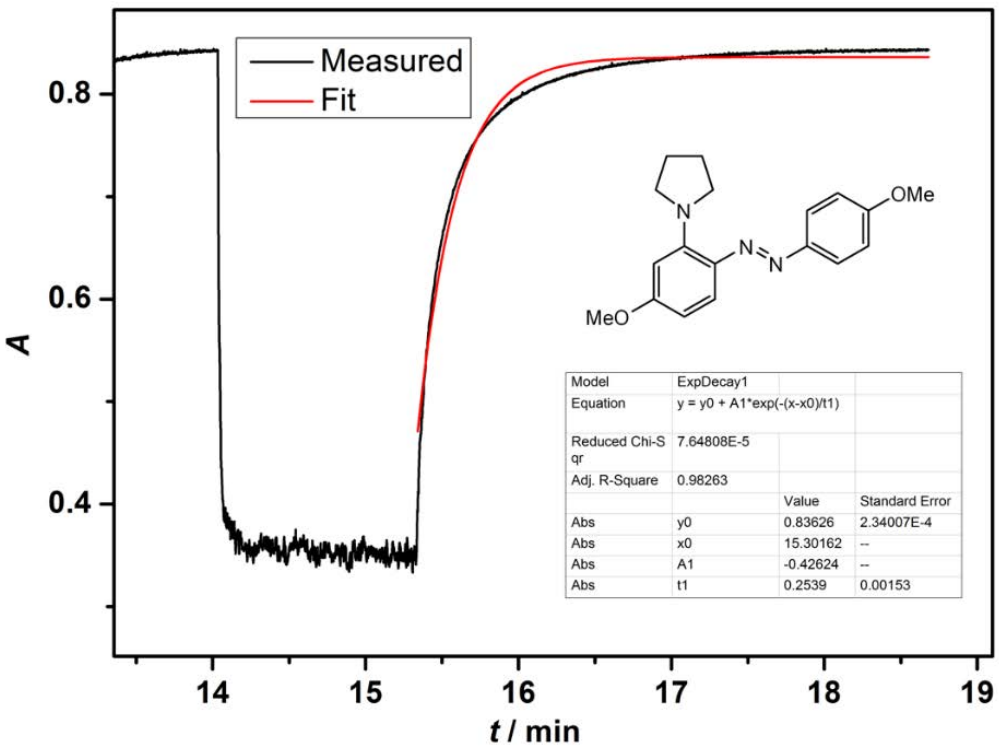

Figure S27. *Cis*-lifetime for compound **4** in kinetic mode at 25°C.

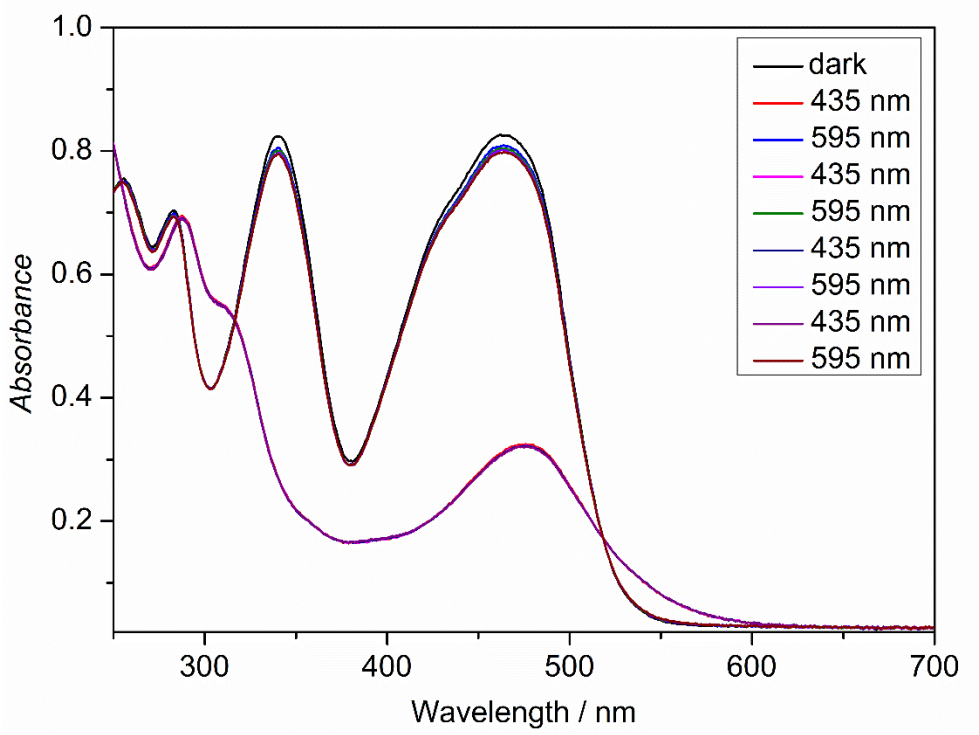

Figure S28. Back and forth switching cycles of **4** using 435 and 595 nm wavelengths.

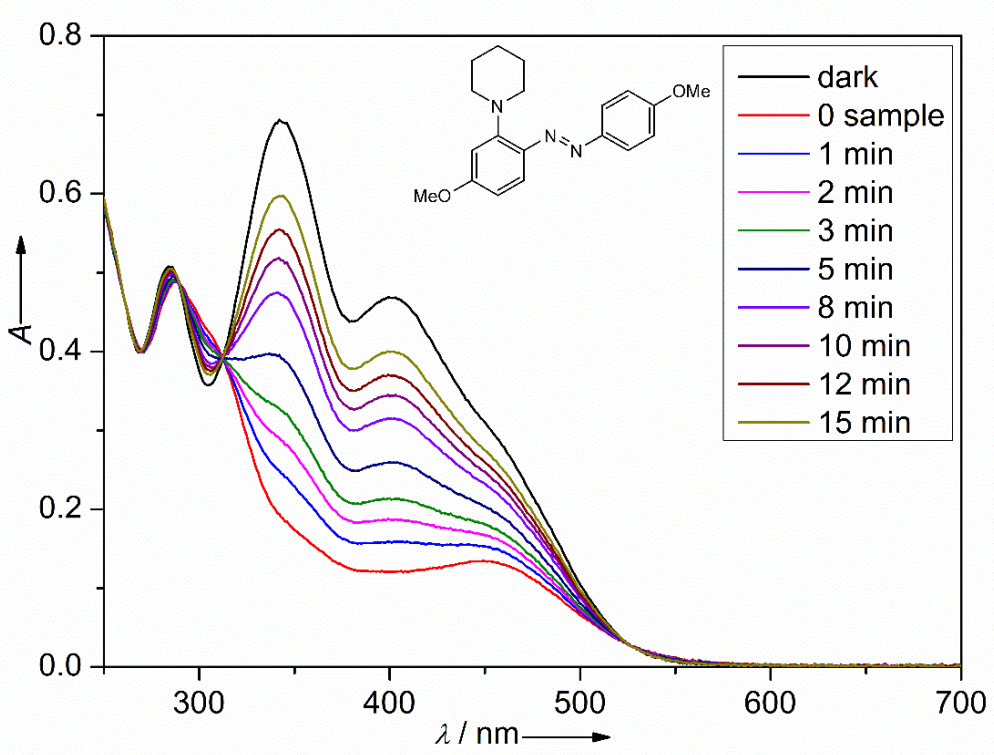

Figure S29. Thermal *cis*-to-*trans* isomerization of compound **5** at 60°C.

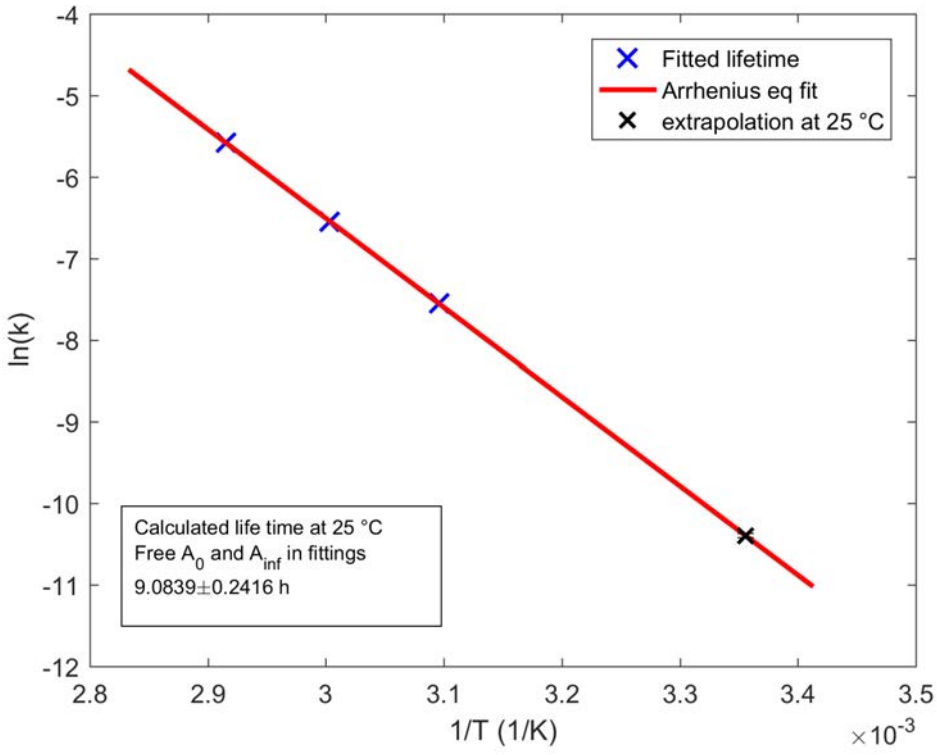

Figure S30. Arrhenius plot of compound **5**.

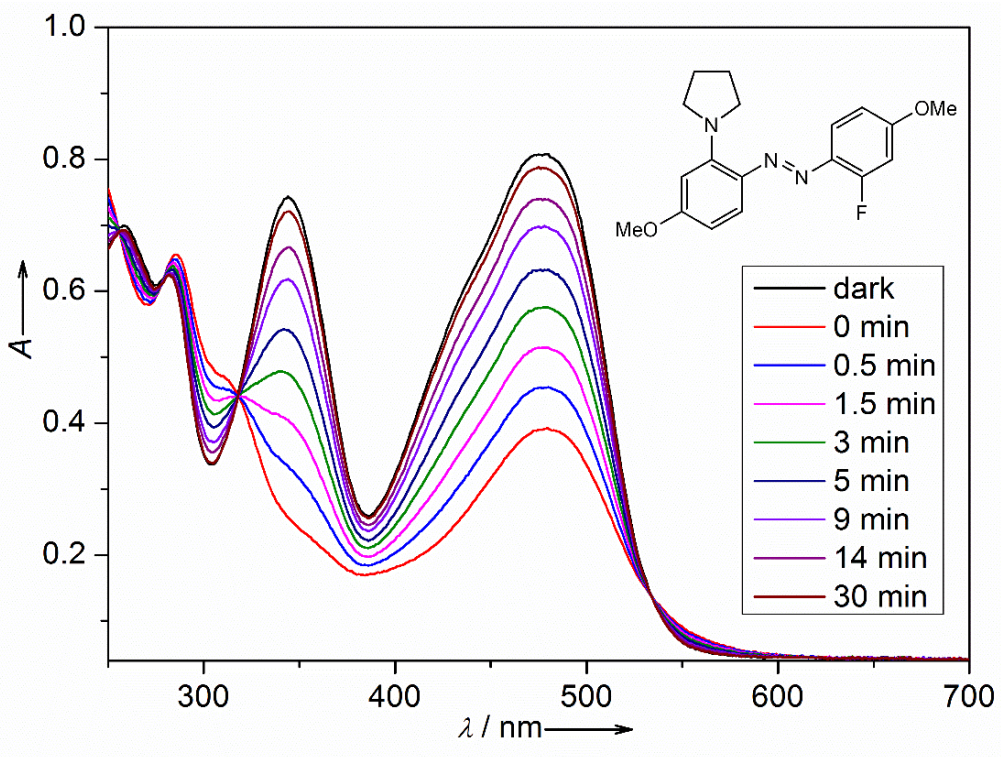

Figure S31. Thermal *cis*-to-*trans* isomerization of compound **6** at 25°C.

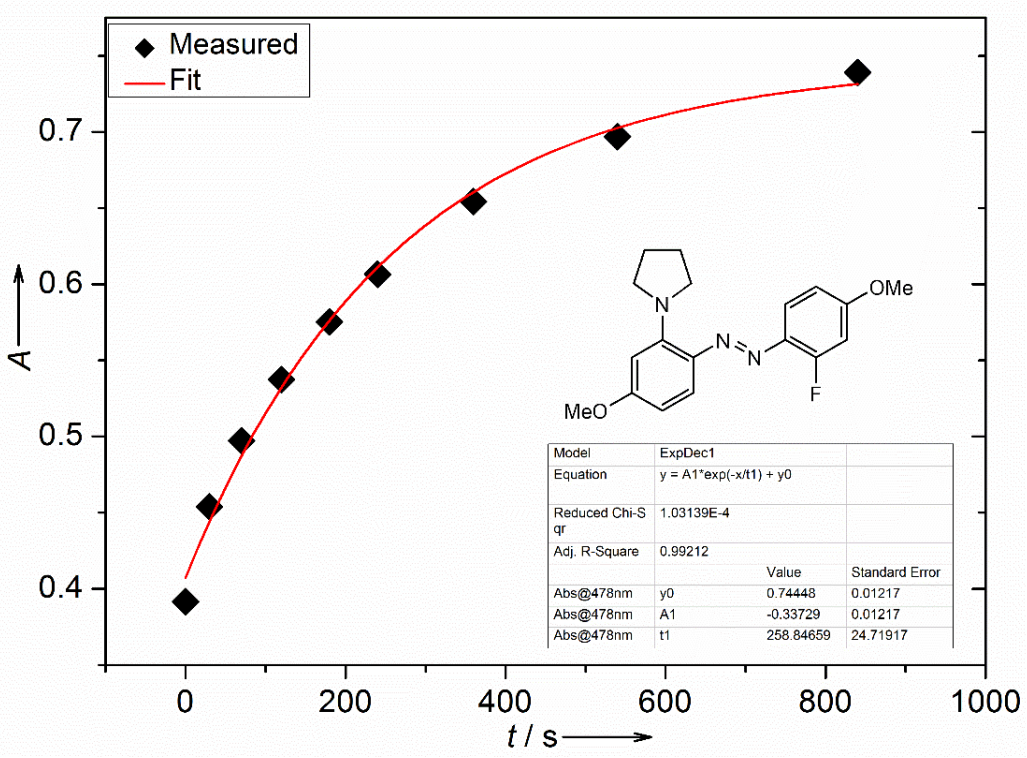

Figure S32. *Cis*-lifetime calculation for compound **6**.

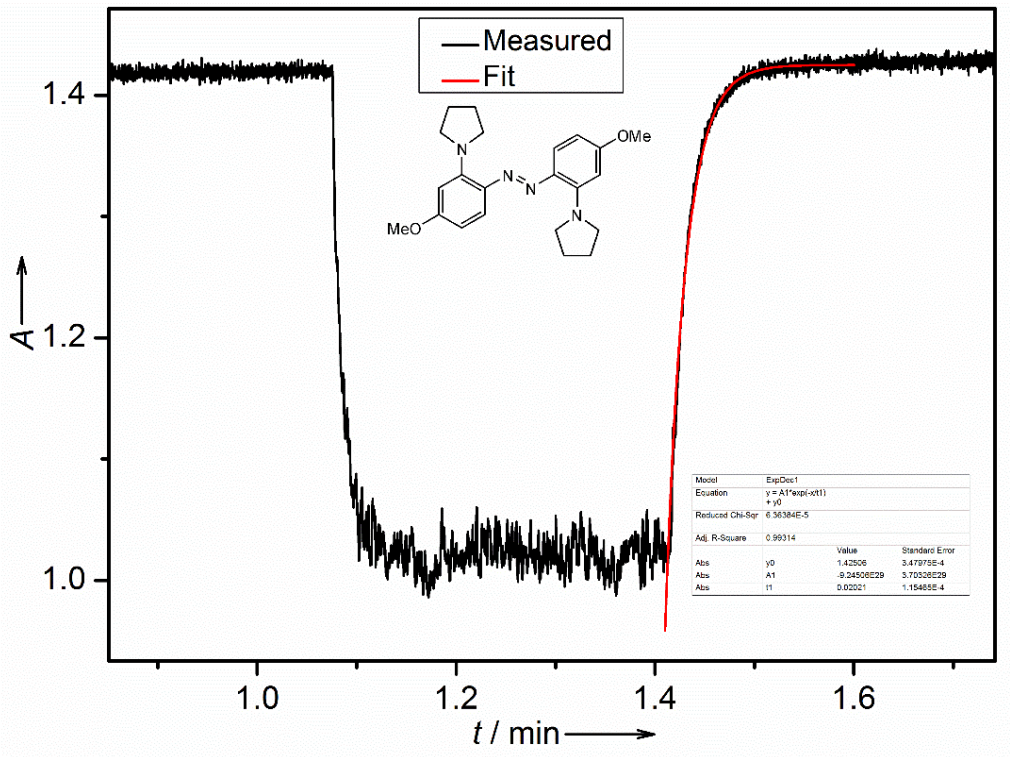

Figure S33. *Cis*-lifetime study for compound **7** in kinetic mode at 25°C.

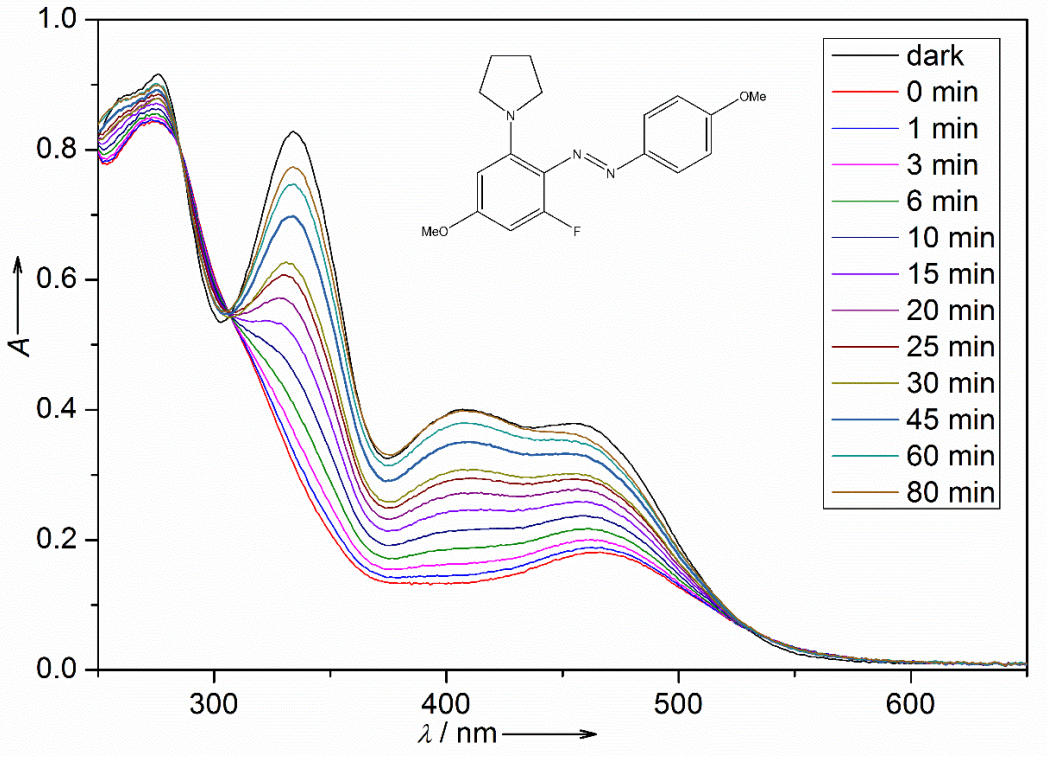

Figure S34. Thermal *cis*-to-*trans* isomerization of compound **9** at 70°C.

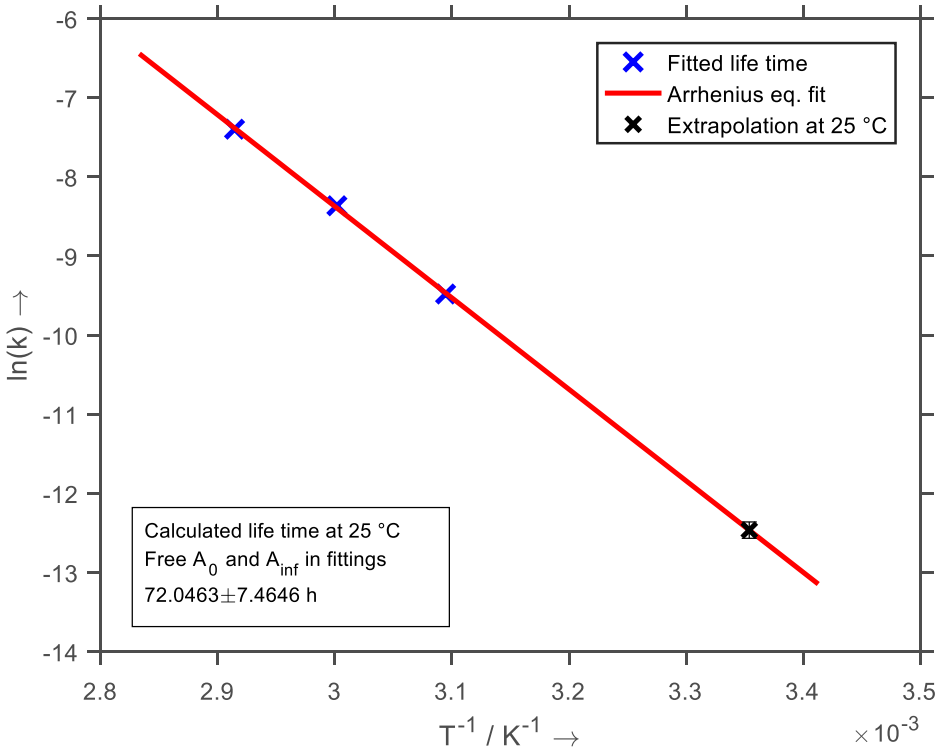

Figure S35. Arrhenius plot of compound **9**.

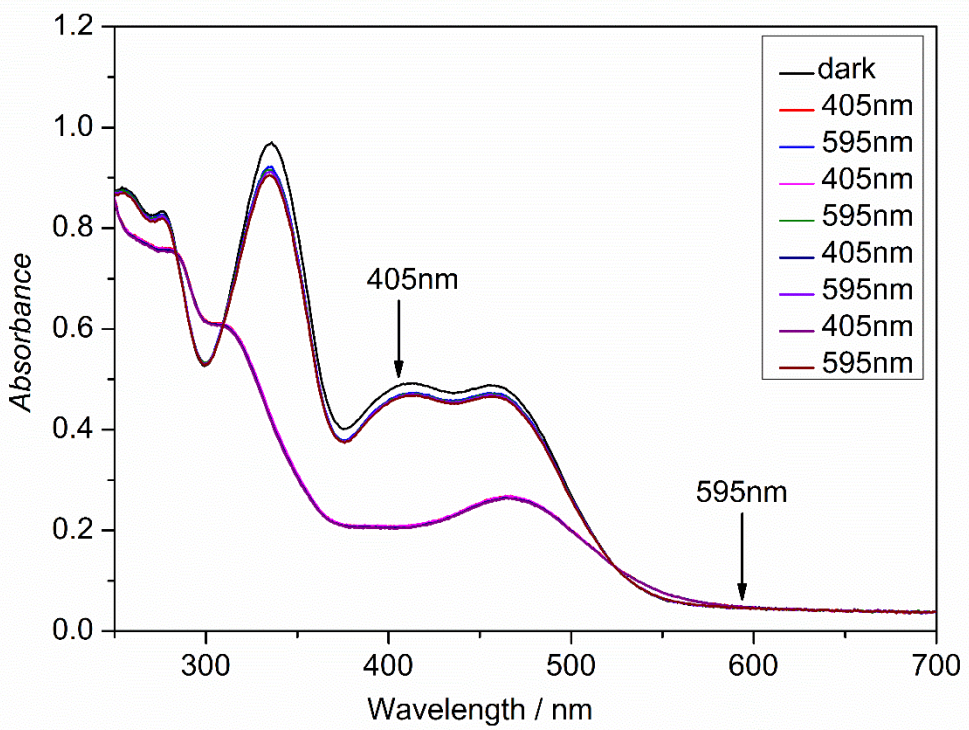

Figure S36. Back and forth switching cycles of **9** using 405 and 595 nm wavelengths.

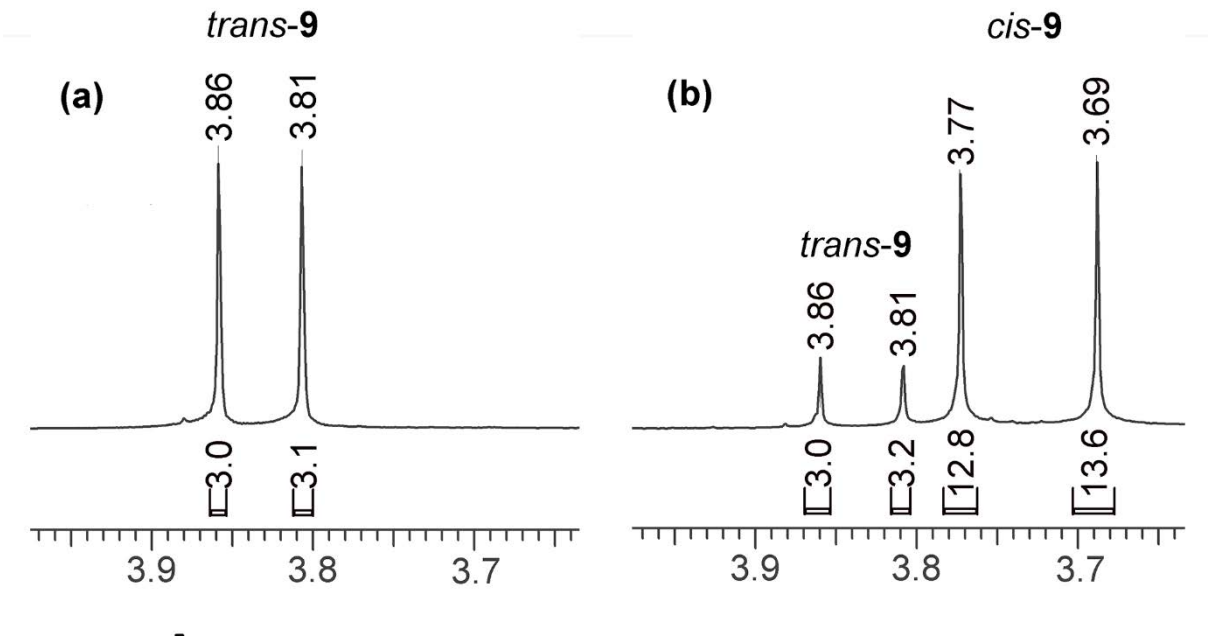

Figure S37. [1]HNMR spectra of compound **9** (expanded methoxy regions) before (a) and after (b) irradiation with 405 nm. Integration of methoxy protons indicates > 80% *trans-cis* conversion.

8. References

[1] C. Knie, M. Utecht, F. Zhao, H. Kulla, S. Kovalenko, A. M. Brouwer, P. Saalfrank, S. Hecht, D. Bleger, *Chem. - Eur. J.* **2014**, *20*, 16492.

[2] M. Poutanen, O. Ikkala, A. Priimagi, *Macromolecules* **2016**, *49*, 4095.